Published OnlineFirst July 27, 2010; DOI:10.1158/0008-5472.CAN-10-0096

effects of ECI301 on peripheral blood. RFA alone had few effects on the numbers of CCR1-expressing cells, but subsequent ECI301 administration increased the numbers of CCR1-expressing cells in peripheral blood, particularly $CD11c^+$ cells, but not $CD4^+$ or $CD8^+$ cells (Fig. 3). Because immune cells need to accumulate in RFA-treated tumors at an early stage to initiate adaptive immune responses, CCR1 expression by tumor-infiltrating cells in RFA-treated tumors was examined 8 hours after treatment. RFA-induced $CD4^+$, $CD8^+$, $CD11c^+$, and $F4/80^+$ cell infiltrations into RFA-treated tumors were greater than those into tumors of untreated mice. Moreover, ECI301 further increased the numbers of $CD4^+$, $CD8^+$, and $CD11c^+$ cells infiltrating into RFA-treated tumors compared with the numbers of these cells infiltrating into tumors treated with RFA alone (Fig. 4A and B). In RFA-treated tumors, most $CD11c^+$ and $F4/80^+$ cells expressed CCR1, whereas few $CD4^+$ and $CD8^+$ cells expressed CCR1 (Fig. 4C). Furthermore, ECI301-induced $CD4^+$, $CD8^+$, and

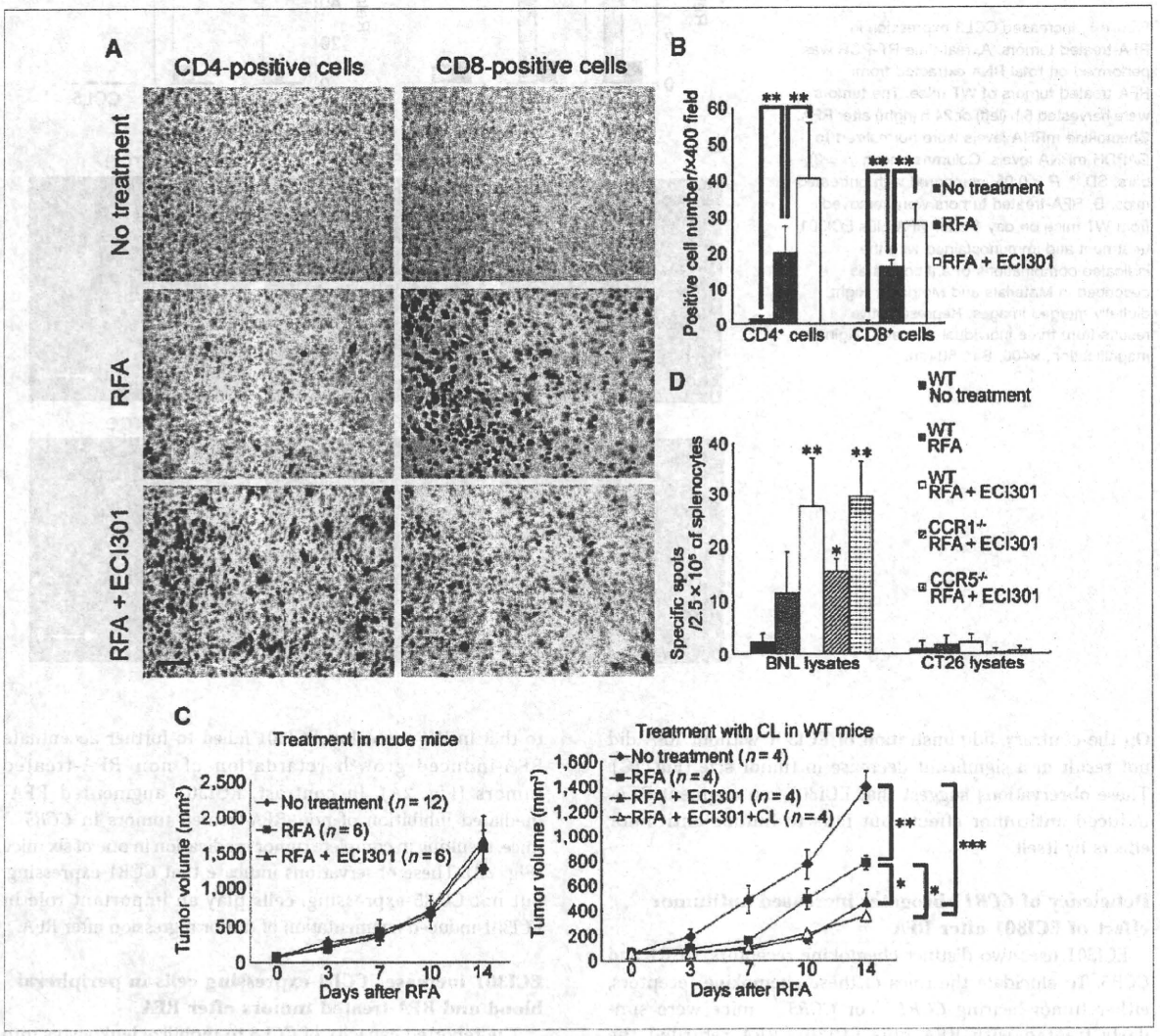

Figure 6. ECI301 augments tumor-specific immune responses after RFA. A, non–RFA-treated tumors were removed from WT mice on day 3 after RFA, and immunohistochemical analysis was done using anti-CD4 or anti-CD8a antibodies. Representative results from three individual animals in each group. Original magnification, ×400. Bar, 50 μm. B, the numbers of $CD4^+$ or $CD8^+$ cells were counted. Cell density was determined in 10 randomly chosen tumor areas at 400-fold magnification. Columns, mean (n = 5); bars, SE. **, $P < 0.01$. C, BALB/c-*nu/nu* mice (left) and BALB/c-WT mice (right) were inoculated with BNL cells and treated as described in the legend to Fig. 1. In the RFA + ECI301 + clodronate liposome (CL) group, the mice were injected with 200 μL of CL to deplete monocytes/macrophages as described in Materials and Methods. Non–RFA-treated tumor volumes were measured twice a week. Points, mean; bars, SE. D, spleens from WT, *CCR1*$^{-/-}$, or *CCR5*$^{-/-}$ mice were harvested on day 21 after RFA, and mononuclear cells were separated from the spleens for ELISPOT assay as described in Materials and Methods. The number of specific spots was determined by subtracting the number of spots in wells without lysates from the number of spots in wells with tumor lysates. Columns, mean (n = 3); bars, SE. *, $P < 0.05$; **, $P < 0.01$, compared with untreated WT mice.

Published OnlineFirst July 27, 2010; DOI:10.1158/0008-5472.CAN-10-0096

$CD11c^+$ cell infiltrations into ablated tumors were lesser in $CCR1^{-/-}$ mice than in WT mice, whereas $F4/80^+$ cells infiltrated RFA-treated tumors in $CCR1^{-/-}$ mice and WT mice to a similar extent (Fig. 4D). These observations suggest that ECI301 augments RFA-induced $CD4^+$, $CD8^+$, and $CD11c^+$ cell infiltrations into RFA-treated tumors in a CCR1-dependent manner.

ECI301 increases intratumoral expression of CCL3 after RFA

We showed that $CCR1^+$ cells were mobilized into blood by i.v. administered ECI301. However, the concentration of ECI301 in blood can go down rapidly as time passes (the peak is 5 minutes, and the half-life is <2 hours),[4] allowing ECI301-mobilized $CCR1^+$ cells to migrate into tissues where chemokines are highly produced. To prove this point, chemokine expression in RFA-treated tumors was examined. RFA plus ECI301 treatment increased *CCL3* mRNA expression level 6 hours after RFA. Moreover, 24 hours after treatment, *CCL3* and *CCL4* mRNA expression levels became almost 10-fold higher in tumors treated with RFA alone than in tumors of untreated mice, and ECI301 further increased the mRNA expression level of these chemokines in RFA-treated tumors (Fig. 5A). CCL3 and CCL4 were detected in tumor-infiltrating $F4/80^+$ cells (Fig. 5B). These observations indicate that RFA treatment causes local production of CCL3 and CCL4 in RFA-treated tumors and ECI301 further increases the expression of these chemokines. As the concentration of ECI301 in blood decreases, chemokines produced locally in RFA-treated tumor can attract CCR1-expressing $CD11c^+$ cells, thereby indirectly inducing CCR1-negative $CD4^+$ and $CD8^+$ cell infiltrations.

ECI301 augments RFA-induced tumor-specific immune responses accompanied by T-cell infiltrations into non–RFA-treated tumors

Non–RFA-treated tumors were analyzed histologically to clarify the mechanisms underlying the CCR1-dependent inhibitory effect of RFA plus ECI301 treatment against these tumors. Although few $CD4^+$ or $CD8^+$ cells were observed in the tumors of untreated mice, RFA treatment increased the numbers of $CD4^+$ and $CD8^+$ cells in the non–RFA-treated tumors 3 days after RFA. ECI301 further augmented RFA-induced $CD4^+$ and $CD8^+$ cell infiltrations into non–RFA-treated tumors (Fig. 6A and B). However, only a marginal number of $CD11c^+$ or $F4/80^+$ cells infiltrated into non–RFA-treated tumors of mice treated with RFA alone or RFA plus ECI301-treated mice (data not shown). Based on these findings, we hypothesized that ECI301-augmented tumor regression after RFA may be associated with T-cell–mediated antitumor immune responses. To clarify this point, *nu/nu* mice on a BALB/c background were treated by RFA with or without ECI301. Deficiency of T cells abrogated the tumor-inhibitory effect of ECI301 as well as the RFA-induced antitumor effect (Fig. 6C). Thus, both ECI301- and RFA-induced tumor regressions require T-cell–mediated antitumor immune response.

[4] Unpublished data from Effector Cell Institute.

However, $CD4^+$ or $CD8^+$ T cells rarely expressed CCR1 in blood and RFA-treated tumors. $CCR1^+$ cells in RFA-treated tumors were $CD11c^+$ cells and $F4/80^+$ cells, and only the former accumulate in RFA-treated tumors in a CCR1-dependent manner. These findings suggest that CCR1-positive $CD11c^+$ cells may activate antitumor T-cell responses and indirectly induce tumor retardation. Accordingly, we next examined the effect of depletion of monocytes/macrophages on ECI301-augmented tumor regression. I.p. injection of clodronate liposome depleted CD11c-negative monocytes in blood, although it did not change the number of $CD11c^+$ cells (data not shown). Depletion of these CD11c-negative monocytes did not cause any effects on ECI301-enhanced tumor regression, indicating that ECI301-augmented antitumor T-cell immunity was independent of CD11c-negative monocytes (Fig. 6C).

Finally, to prove the presence of systemic adaptive immune responses, IFN-γ ELISPOT assay was performed using mononuclear cells from the spleen. A greater number of spots against BNL cell lysates, but not against CT26 cell lysates, were generated by RFA plus ECI301–treated mice than that by mice treated with RFA alone or untreated mice. Moreover, ablation of *CCR1* gene, but not *CCR5* gene, reduced the number of spots against BNL cell lysates even when the mice were treated with RFA plus ECI301 (Fig. 6D). These observations suggest that ECI301 can further augment RFA-induced tumor-specific adaptive immune responses and subsequent tumor retardation in a CCR1-dependent manner.

Discussion

HCC occurs predominantly in individuals with chronic liver disease related to hepatitis B or hepatitis C virus infections (22–24). In addition to surgical resection, RFA treatment has been developed to eradicate solitary HCC lesions (25). RFA of HCC induces specific T-cell responses against liver tumors in human and rabbit (8, 11). Moreover, activated dendritic cells were detected in peripheral blood of HCC patients after RFA (9). These previous reports indicate that RFA treatment can induce antitumor immune responses against HCC (8–11). Likewise, we observed that RFA treatment generated tumor-specific IFN-γ–producing cells and inhibited the growth of non–RFA-treated tumors accompanied by massive T-cell infiltration into these tumors. However, even after successful ablation of HCC lesion by RFA, tumor recurrence often occurs probably because HCC develops in a multicentric manner in the cirrhotic liver (12). These observations indicate that RFA-induced augmentation in immune response may not be sufficient to prevent tumor recurrence. Thus, a novel therapeutic modality is required to further augment RFA-induced tumor-specific immune responses. Here, we showed that combined administration of ECI301 and RFA can augment tumor-specific immune responses against HCC.

Several chemokines are used for immunotherapy against cancers because they can attract immune cells such as dendritic and cytotoxic T cells to augment tumor-specific immune responses (26). However, some chemokines can simultaneously attract myeloid-derived suppressor and regulatory T cells to promote neovascularization and induce immunosuppressive

Published OnlineFirst July 27, 2010; DOI:10.1158/0008-5472.CAN-10-0096

microenvironments (26–28). The double-edged activities of chemokines frequently preclude their use for tumor immunotherapy. Moreover, most chemokines exhibit a bell-shaped dose-response curve with a narrow effective dose window. Thus, determination of an optimal dose of chemokines is important to elicit efficient antitumor responses (29). Several lines of evidence show that intratumoral use of CCL3 reduces tumorigenicity (6, 30). Furthermore, there are no reports showing that use of CCL3 can promote tumor progression. We observed that systemic administration of ECI301 without RFA treatment induced neither reduction nor progression of tumors. On the contrary, systemic injection of ECI301 after RFA can inhibit the growth of non–RFA-treated tumors in the contralateral side. ECI301-enhanced tumor regression after RFA was both CCR1 and T-cell dependent, but T cells rarely expressed CCR1 in blood and RFA-treated tumors. Because depletion of monocytes/macrophages did not affect the retardation of ECI301-treated tumors, CCR1-expressing $CD11c^+$ dendritic cells might activate antitumor T-cell responses and indirectly induce tumor retardation via some mechanisms such as antigen presentation and cytokine production. ECI301 mobilized a large number of $CCR1^+$ cells into blood, and these mobilized cells may be attracted into highly CCL3-producing RFA-treated tumors and cause increased number of tumor-infiltrating $CCR1^+CD11c^+$ dendritic cells. Thus, $CCR1^+$ precursors in blood and $CCR1^+CD11c^+$ tumor-infiltrating dendritic cells might play important roles in ECI301-augmented antitumor effects (31–33).

ECI301 could not increase the number of $F4/80^+$ cells in the RFA-treated tumor sites. Accumulation of $F4/80^+$ cells in the tumor treated with ECI301 plus RFA was also independent of CCR1. $F4/80^+$ cells, which might include a large number of macrophages/monocytes, are usually attracted into the tumor by CCL2, CCL4, and CCL5 that are produced in the tumor sites. CCR2, the receptor for CCL2, and CCR5, the receptor for CCL4 and CCL5, might be responsible for migration of monocytes/macrophages (27, 34–36). However, it is still unclear whether monocytes/macrophages use CCR2 or CCR5 after massive tumor cell death caused by treatments such as RFA because tumor cell death induces different profiles of chemokine production in the tumors (4). Although ECI301 did not directly induce migration of $F4/80^+$ cells, the mechanism underlying the infiltration of $F4/80^+$ macrophages remains to be elucidated.

Breaking tolerance for tumor cells is necessary for induction of antitumor immunity. Several independent groups have suggested multiple mechanisms underlying immunogenic tumor cell death induced by anticancer chemotherapy or radiation therapy (37–40). Anthracyclin causes apoptosis along with translocation of calreticulin to the apoptotic tumor cell surface. Calreticulin exposure augments phagocytosis of apoptotic cancer cells by dendritic cells with an eventual increase in immune response (37, 38). Chemotherapy or irradiation kills tumor cells to release high mobility group box 1 (HMGB1). Released HMGB1 activates dendritic cells after binding to toll-like receptor 4 expressed by these cells (39). Apoptosis induced by local radiation therapy augments MHC class I expression by tumor cells, thereby facilitating their recognition by cytotoxic T cells (40). RFA induces the expression of heat shock proteins 70 and 90 on ablated tumor cells, and these proteins can activate toll-like receptor–expressing antigen-presenting cells (41, 42). In addition, we showed that RFA treatment alone caused local production of CCL3 in RFA-treated tumors accompanied by accumulation of T cells and $CD11c^+$ dendritic cells. These mechanisms may also account for the observed RFA-induced generation of tumor-specific immune responses.

We revealed that combined treatment of ECI301 and RFA augmented antitumor-specific immune responses, thereby inhibiting the growth of non–RFA-treated tumors in a CCR1-dependent manner. Thus, combined treatment of ECI301 and RFA can prevent human HCC from recurring after RFA treatment. The absence of any severe adverse effects in mice (data not shown) further warrants the clinical trial of ECI301 combined with RFA as a treatment regimen for HCC.

Disclosure of Potential Conflicts of Interest

No potential conflicts of interest were disclosed.

Acknowledgments

We thank Dr. Philip M. Murphy (National Institute of Allergy and Infectious Disease, NIH) and Dr. Kouji Matsushima (Tokyo University) for providing us with $CCR1^{-/-}$ and $CCR5^{-/-}$ mice, respectively.

The costs of publication of this article were defrayed in part by the payment of page charges. This article must therefore be hereby marked *advertisement* in accordance with 18 U.S.C. Section 1734 solely to indicate this fact.

Received 01/11/2010; revised 06/01/2010; accepted 06/20/2010; published OnlineFirst 07/27/2010.

References

1. Luster AD. Chemokines—chemotactic cytokines that mediate inflammation. N Engl J Med 1998;338:436–45.
2. Castellino F, Huang AY, Altan-Bonnet G, Stoll S, Scheinecker C, Germain RN. Chemokines enhance immunity by guiding naïve $CD8^+$ T cells to sites of $CD4^+$ T cell-dendritic cell interaction. Nature 2006;440:890–5.
3. Sozzani S. Dendritic cell trafficking: more than just chemokines. Cytokine Growth Factor Rev 2005;16:581–92.
4. Iida N, Nakamoto Y, Baba T, et al. Tumor cell apoptosis induces tumor-specific immunity in a CC chemokine receptor 1-and 5-dependent manner in mice. J Leukoc Biol 2008;84:1001–10.
5. Tsuchiyama T, Nakamoto Y, Sakai Y, et al. Prolonged, NK cell-mediated antitumor effects of suicide gene therapy combined with monocyte chemoattractant protein-1 against hepatocellular carcinoma. J Immunol 2007;178:574–83.
6. Crittenden M, Gough M, Harrington K, Olivier K, Thompson J, Vile RG. Expression of inflammatory chemokines combined with local tumor destruction enhances tumor regression and long-term immunity. Cancer Res 2003;63:5505–12.
7. Furumoto K, Soares L, Engleman EG, Merad M. Induction of potent antitumor immunity by *in situ* targeting of intratumoral DCs. J Clin Invest 2004;113:774–83.

THE JOURNAL OF GENE MEDICINE
J Gene Med 2010;12: 1002–1013.
Published online in Wiley Online Library (wileyonlinelibrary.com) DOI: 10.1002/jgm.1528

RESEARCH ARTICLE

Prevention of intrahepatic metastasis of liver cancer by suicide gene therapy and chemokine ligand 2/monocyte chemoattractant protein-1 delivery in mice

Kaheita Kakinoki[1]
Yasunari Nakamoto[1]
Takashi Kagaya[1]
Tomoya Tsuchiyama[1]
Yoshio Sakai[1]
Tohru Nakahama[1]
Naofumi Mukaida[2]
Shuichi Kaneko[1]*

[1]*Disease Control and Homeostasis, Graduate School of Medical Science, Kanazawa University, Kanazawa, Japan*

[2]*Division of Molecular Bioregulation, Cancer Research Institute, Kanazawa University, Kanazawa, Japan*

*Correspondence to:
Shuichi Kaneko, Disease Control and Homeostasis, Graduate School of Medical Science, Kanazawa University, 13-1 Takara-machi, Kanazawa 920-8641, Japan
E-mail: skaneko@m-kanazawa.jp

Received: 22 June 2010
Revised: 28 October 2010
Accepted: 5 November 2010

Abstract

Background The prognosis of patients with hepatocellular carcinoma (HCC) remains poor, largely as a result of intrahepatic metastasis. Using a mouse model of intrahepatic metastasis, we investigated whether chemokine ligand 2/monocyte chemoattractant protein-1 (CCL2/MCP-1) could potentiate the antitumor effects of the herpes simplex virus thymidine kinase/ganciclovir (HSV-tk/GCV) system.

Methods Mouse hepatoma cells infected with recombinant adenovirus vectors expressing HSV-tk, CCL2/MCP-1 and LacZ at multiplicities of infection of Ad-tk/Ad-MCP1 = 3/0.03 (T/M^{Low}), 3/3 (T/M^{High}) and Ad-tk/Ad-LacZ = 3/3 (T/L) were injected into BALB/c mice.

Results Intrahepatic tumor growth was significantly lower in T/M^{Low} mice. By contrast, no tumor suppression was observed in T/M^{High} mice. The tumor-specific cytolytic activities of splenocytes from T/M^{Low} and T/M^{High} mice were comparable. Immunohistochemical analysis of liver tissues showed similar infiltration by Mac-1^+ and T cells in these animals, whereas the proportions of classical activated (M1) monocytes/macrophages were significantly higher in T/M^{Low} mice. In addition, interleukin-12 production was elevated in these tissues. Vascular endothelial growth factor-A expression and $CD31^+$ microvessels were increased in T/M^{High} mice.

Conclusions Collectively, these results demonstrate that an adequate amount of CCL2/MCP-1, together with the HSV-tk/GCV system, may induce T helper 1-polarized antitumor effects without inducing tumor angiogenesis in the microenvironment of intrahepatic HCC progression. Copyright © 2010 John Wiley & Sons, Ltd.

Keywords chemokines; hepatocellular carcinoma; monocytes/macrophages

Introduction

Primary liver cancer is the fifth most common neoplasm in the world and the third most common cause of cancer-related deaths [1,2]. Despite the development of novel modalities for the treatment of hepatocellular carcinoma (HCC), including transcatheter arterial embolization, percutaneous ablation, surgical resection and liver transplantation, the prognosis of patients with HCC still remains relatively poor. One of the major factors responsible for

these unsatisfactory outcomes is the high frequency of intrahepatic recurrence after curative treatment [1,2]. Intrahepatic recurrence is the result of two mechanisms: intrahepatic metastasis (IM) originating from the primary cancer, and a second primary cancer arising from multicentric carcinogenesis (MC). IM may correlate with early recurrence and poor prognosis, whereas MC is associated with relatively good prognosis [3–5].

To develop novel antitumor strategies for HCC, we have investigated the effectiveness of immune gene therapy using suicide genes and chemokine molecules, including chemokine ligand 2/monocyte chemoattractant protein-1 (CCL2/MCP-1) [6–8]. CCL2/MCP-1 is a chemokine that regulates the recruitment of monocytes/macrophages to inflammatory sites and tumor tissues, as well as their activation, including lysosomal enzyme release and tumoricidal activity, and is functional in both mice and humans [9]. Transfectant-derived CCL2/MCP-1 has been found to successfully recruit monocytes into tumor tissue [10,11]. We recently described a combination strategy for the treatment of HCC, consisting of the herpes simplex virus thymidine kinase/ganciclovir (HSV-tk/GCV) system and CCL2/MCP-1 gene delivery. We found that adenovirally delivered CCL2/MCP-1 enhanced the antitumor effects of the HSV-tk/GCV system by activating innate immune responses involving monocytes/macrophages, as well as demonstrating prolonged efficacy mediated by natural killer cells [6–8]. These experiments were performed in athymic nude mice, deficient in acquired immune responses, subcutaneously transplanted with HCC.

In the present study, we have used a liver metastasis model, in which tumor cells were infused through the portal vein (PV), to investigate whether CCL2/MCP-1 gene delivery could potentiate the antitumor effects of the suicide gene system. The results obtained indicate that the antitumor effects of the suicide gene are enhanced by codelivery of an adequate amount of CCL2/MCP-1. These antitumor effects were associated with the recruitment of monocytes/macrophages and T cells, T helper 1 (Th1) cytokine gene expression and the induction of splenocyte cytolytic activity. These findings indicate that CCL2/MCP-1 has an immunomodulatory effect on suicide gene therapy for HCC by orchestrating the innate and acquired immune responses.

Materials and methods

Animals

Male BALB/cA Jcl mice, 6–8 weeks of age, were obtained from CLEA Japan Inc. (Tokyo, Japan), maintained at constant room temperature (25 C) and provided with free access to standard diet and tap water throughout, in accordance with institutional guidelines.

Cell lines and cell culture

The mouse HCC cell line BNL 1ME A.7R.1 (BNL) and the mouse colon cancer cell line colon 26 clone 20 (CT 26), derived from BALB/c mice (H-2d), were cultured in Dulbecco's modified Eagle's medium supplemented with 10% heat-inactivated (30 min at 56 C) fetal bovine serum (FBS), non-essential amino acids, sodium pyruvate, HEPES buffer, 2 mM glutamate, 1 mM penicillin/streptomycin and 0.2 mM gentamicin (Gibco, Long Island, NY, USA) at 37 °C in 5% CO_2.

Recombinant adenovirus vectors

The following replication-defective adenovirus vectors, driven by the CAG promoter [12], were prepared by recombinant DNA technology: Ad-tk, which expresses the HSV-tk gene; Ad-MCP1, which expresses the human CCL2/MCP-1 gene; and Ad-LacZ, which expresses the LacZ gene [13] (Figure 1A). Each recombinant adenovirus vector was purified and titered according to protocols supplied by the manufacturer (Takara, Ootsu, Japan). Briefly, each gene fragment (i.e. HSV-tk, CCL2/MCP-1 and LacZ) was excised from its respective insert-containing pBluescript vector and inserted into the cosmid pAxCA-wt (Takara, Ootsu, Japan), which contains essentially the full-length adenovirus type 5 genome apart from the E1 and E3 regions, thus generating the pAxCA gene (Figure 1A). The recombinant adenovirus vectors (rAds) were generated by transfecting 293 cells with pAxCA-gene and adenovirus 5-dIX DNA-terminal protein complex. These rAds were propagated in 293 cells [14], and viral stocks were prepared by standard protocols [15]. The titers of rAds were determined by the 50% tissue culture infectious dose ($TCID_{50}$) method [16].

Enzyme-linked immunosorbent assay (ELISA) for CCL2/MCP-1

Aliquots of 2.5×10^4 BNL cells were seeded in 3.0 ml of culture media in six-well tissue culture plate. After 24 h, the cells were infected with Ad-MCP1 and Ad-MCP1, together with Ad-tk, at various multiplicities of infections (MOIs). After 24 h, the media were collected from the wells, and the concentrations of CCL2/MCP-1 were determined by ELISA. Briefly, each well of a 96-well microtiter plate (Nalgene, Rochester, NY, USA) was coated with 0.05 M carbonate buffer (pH 9.6) containing monoclonal anti-human CCL2/MCP-1 antibody (ME 6.1; 1 μg/ml) overnight at 4 C. After washing with phosphate-buffered saline (PBS) containing 0.05% Tween 20, the plates were blocked with PBS containing 1% bovine serum albumin for 1 h at 37 C. Diluted culture medium or various concentrations of recombinant CCL2/MCP-1 were added to duplicate wells and incubated for 2 h at 37 C. The plates were washed, incubated with rabbit anti-CCL2/MCP-1 antibodies (1 μg/ml) for 2 h at 37 C,

J Gene Med 2010;**12**: 1002–1013.
DOI: 10.1002/jgm

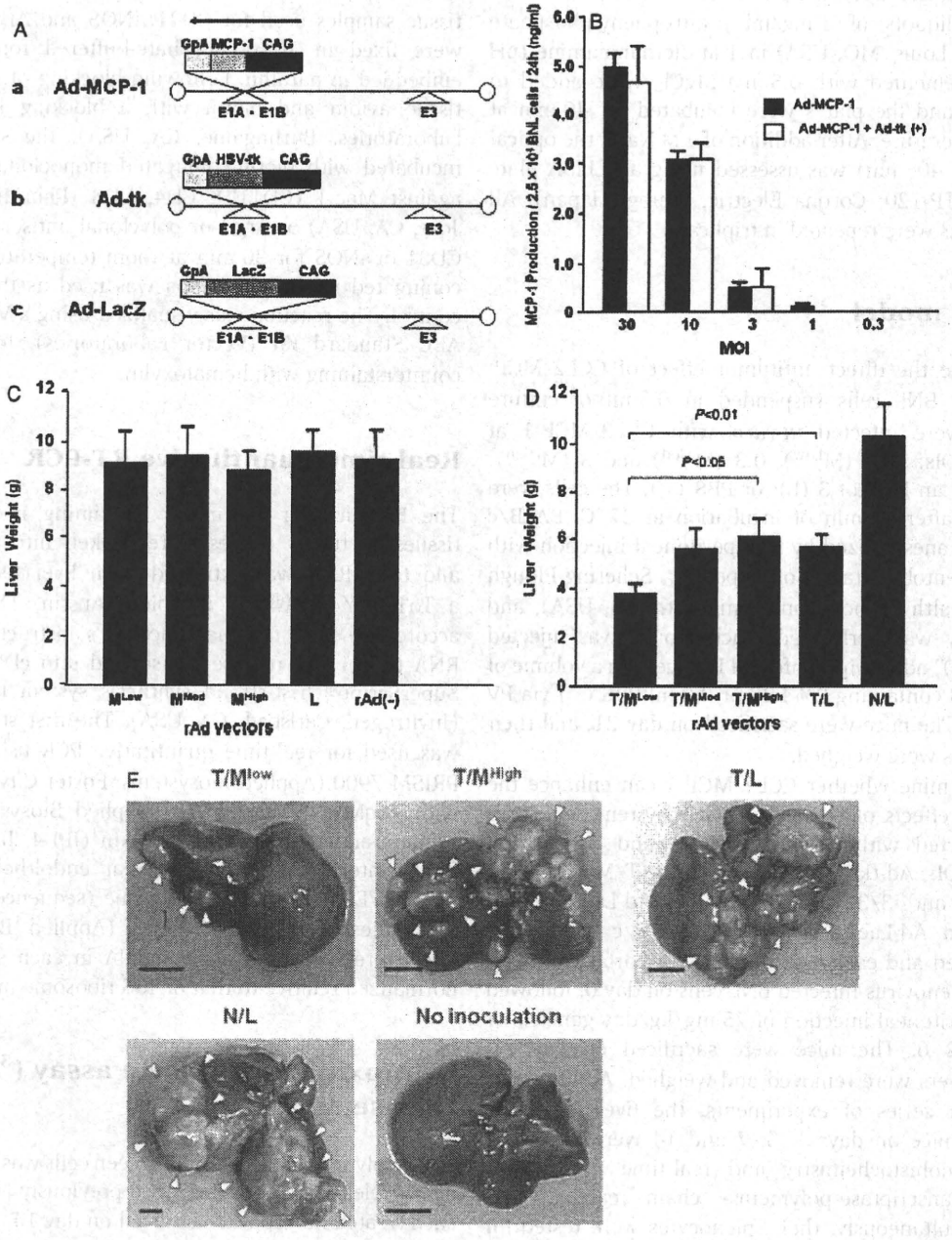

Figure 1. CCL2/MCP-1 production and antitumor effects of rAds. (A) Schematic representation of rAds expressing each gene under the control of a CAG promoter. (a) Ad-MCP1 expressing CCL2/MCP-1. (b) Ad-tk expressing HSV-tk. (c) Ad-LacZ expressing β-galactosidase gene (LacZ). Solid lines indicate the rAd genome, and the open triangle below each rAd genome represents the deletion of adenovirus early regions. The arrow shows the orientation of transcription. GpA, rabbit β-globin (A) site; CAG, CAG promoter. (B) Production of CCL2/MCP-1 by BNL cells infected with rAds at various MOIs. The CCL2/MCP-1 concentrations in culture supernatants were determined by ELISA. Data shown are the mean $\pm$ SE of three independent results. (C) Liver weight following transfer of BNL cells infected with Ad-MCP1, Ad-LacZ or PBS (–). Each mouse was injected via the PV with 1×10^6 BNL cells infected with Ad-MCP1 at various MOIs: 0.03 (M^{Low}), 0.3 (M^{Mod}) and 3 (M^{High}), and Ad-LacZ at the MOI of 3 (L), and the whole livers were weighed on day 21. (D) CCL2/MCP-1 enhancement of the antitumor effects of the HSV-tk/GCV system against intrahepatic cancer cells. Each mouse was injected via the PV with BNL cells (1×10^6) infected with Ad-tk, Ad-MCP1 and Ad-LacZ at various MOIs: Ad-tk/Ad-MCP1 = 3/0.03 (T/M^{Low}), 3/0.3 (T/M^{Mod}) and 3/3 (T/M^{High}); Ad-tk/Ad-LacZ = 3/3 (T/L); and Ad-LacZ = 6 (N/L), and the whole livers were weighed on day 21. (E) The macroscopic views of hepatic tumors (open arrowheads) in mice. Tumor growth was markedly suppressed in T/M^{Low} mice. Scale bars = 10 mm

washed again and incubated with alkaline phosphatase-conjugated goat anti-rabbit antibody (1:12 000; Tago, Burlingame, CA, USA) for 2 h at 37 C. The plates were washed, aliquots of 1 mg/ml *p*-nitrophenylphosphate (Sigma, St Louis, MO, USA) in 1 M diethanolamine (pH 9.8) supplemented with 0.5 mM $MgCl_2$ were added to the wells, and the plates were incubated for 40 min at room temperature. After addition of 1 M NaCl, the optical density (at 405 nm) was assessed using an ELISA plate reader (MTP-120; Corona Electric, Ibaragi, Japan). All experiments were repeated in triplicate.

Disease model

To evaluate the direct antitumor effect of CCL2/MCP-1, 1×10^7 BNL cells suspended in 0.5 ml of culture medium were infected *in vitro* with CCL2/MCP-1 at various MOIs: 0.03 (M^{Low}), 0.3 (M^{Mod}) and 3 (M^{High}); Ad-LacZ at an MOI of 3 (L); or PBS ( ). The cells were harvested after 30 min of incubation at 37 C. BALB/c mice were anesthetized by intraperitoneal injection with sodium pentobarbital (Somnopentyl, Schering-Plough Animal Health Corporation, Kenilworth, NJ, USA), and laparotomy was performed. Each mouse was injected with 1×10^6 adenovirus-infected BNL cells in a volume of 0.2 ml PBS containing 2% FBS or 0.2 ml PBS ( ) via PV on day 0. The mice were sacrificed on day 21, and their liver tissues were weighed.

To determine whether CCL2/MCP-1 can enhance the antitumor effects of the HSV-tk/GCV system, BNL cells were infected with Ad-tk, Ad-MCP1 and Ad-LacZ at various MOIs: Ad-tk/Ad-MCP1 = 3/0.03 (T/M^{Low}), 3/0.3 (T/M^{Mod}) and 3/3 (T/M^{High}); Ad-tk/Ad-LacZ = 3/3 (T/L); and Ad-LacZ = 6 (N/L). BALB/c mice were anesthetized and each was injected via portal vein with 1×10^6 adenovirus-infected BNL cells on day 0, followed by intraperitoneal injection of 75 mg/kg/day ganciclovir on days 2–6. The mice were sacrificed on day 21, and the livers were removed and weighed. Additionally, in another series of experiments, the livers removed from the mice on days 1, 3, 7 and 14 were processed for immunohistochemistry and real-time quantitative reverse transcriptase-polymerase chain reaction (RT-PCR). Simultaneously, their splenocytes were tested for cytolytic activity against ^{51}Cr-labeled BNL cells.

Histopathological and immunohistochemical analysis

Liver sections were fixed in 10% zinc-buffered formalin and stained with hematoxylin and eosin (H&E). For histological evaluation, mouse livers were harvested, embedded in tissue-Tek® OCT embedding medium (Sakura Finetek, Torrance, CA, USA) and stored at 80 C until use, except those stained for CD31 (Abcam, Cambridge, MA, USA), arginase I (Arg I; BD Biosciences, Franklin Lakes, NJ, USA) and inducible nitric oxide synthase (iNOS; Thermo Fisher Scientific, Fremont, CA, USA). Cryostat sections of frozen tissues were fixed in cold acetone for 10 min and rinsed three times with PBS. The tissue samples used for CD31, iNOS and Arg I staining were fixed in 10% phosphate-buffered formalin and embedded in paraffin. Following blocking of nonspecific tissue avidin and biotin with a blocking kit (Vector Laboratories, Burlingame, CA, USA), the slides were incubated with biotin-conjugated monoclonal antibody against Mac-1 (CD11b), CD4, CD8 (PharMingen, San Jose, CA, USA) or Arg-I or polyclonal antiserum against CD31 or iNOS for 30 min at room temperature. Biotin-conjugated rat IgG2b, kappa was used as the negative control. The reaction was visualized using a Vectastain® ABC Standard Kit (Vector Laboratories), followed by counterstaining with hematoxylin.

Real-time quantitative RT-PCR

The Frozen liver specimens containing necrotic liver tissues or tumor tissues were broken into fine pieces and total RNA was extracted from liver tissues using a ToTALLY RNA® kit (Ambion, Austin, TX, USA) in accordance with the manufacturer's instructions. Total RNA (1 µg) was reverse transcribed into cDNA using a SuperScript® first-strand synthesis system for RT-PCR (Invitrogen, Carlsbad, CA, USA). The first strand cDNA was used for real-time quantitative PCR using the ABI PRISM 7900 (Applied Biosystems, Foster City, CA, USA) with TaqMan® Master Mix (Applied Biosystems), and primers and probes for interleukin (IL)-4, IL-10, IL-12, IL-18, interferon (IFN)γ, vascular endolthelial growth factor (VEGF)-A and 18S ribosome (sequences available on request from the authors) (Applied Biosystems). The expression of cytokine mRNA in each sample was normalized relative to that of 18S ribosome mRNA.

Cytotoxic T lymphocyte assay (^{51}Cr release assay)

The cytolytic activity of mouse spleen cells was assessed by a ^{51}Cr release assay, as described previously [17]. Briefly, each treated mouse was sacrificed on day 14, splenocytes were harvested aseptically and mashed in alpha-minimal essential medium (MEM) medium (Gibco) with 10% FBS, and suspensions of single spleen cells were prepared. Spleen cells were cultured with mitomycin C (MMC; Sigma) (400 µg/4 ml, 1 mg/ml in HBSS) treated BNL or CT26 cells in complete alpha-MEM medium containing 10% FBS and 2.5% EL-4 culture supernatant (a source of T cell growth factor) for 5 days. Target cells consisted of 3×10^5 BNL cells labeled with 0.3 mCi $Na_2{}^{51}CrO_4$ (NEN Life Science Products, Boston, MA, USA) at 37 C for 1 h. Effector spleen cells were incubated with 5×10^3 target cells in 96-well plates at various effector/target ratios for 4 h at 37 C, and the ^{51}Cr released into the culture supernatants was quantified by scintillation

counting. Percent specific cytotoxicity was calculated according to the equation: [100 × (experimental release − spontaneous release)/(maximum release − spontaneous release)]. Spontaneous release was defined as the ^{51}Cr in the supernatant of target cells incubated for 4 h, and maximum release was defined as ^{51}Cr in the supernatant of target cells treated with 2% Triton-X. Experiments were performed three times and the results expressed as the mean ± SE. Tumor specificity was determined based on differences between BNL and CT 26 cells. All results presented are the means of triplicate assays.

Results

CCL2/MCP-1 production of recombinant adenoviruses *in vitro*

The production of CCL2/MCP-1 was evaluated by measuring the concentrations in culture media of BNL cells infected with varying MOIs of Ad-MCP1 and Ad-MCP1 plus Ad-tk by ELISA (Figure 1B). The production of CCL2/MCP-1 by cells infected with Ad-MCP1 increased in proportion to the MOI. Importantly, its production by Ad-MCP1 infected cells was not changed when these cells were further infected with Ad-tk (Ad-MCP1 plus Ad-tk), indicating that CCL2/MCP-1 production by Ad-MCP1 was not influenced by coinfection with Ad-tk in BNL cells. In addition, the functional properties of CCL2/MCP-1 produced by this rAd were defined previously [6–8].

Intrahepatic tumor development following transfer of HCC cells infected with recombinant adenoviruses

To evaluate the direct antitumor effect of CCL2/MCP-1 in an immunocompetent mouse model of IM, mice were injected via the PV with BNL cells infected with Ad-MCP1 or Ad-LacZ at various MOIs (Figure 1C). When whole livers were weighed on day 21, the weights of M^{Low} ($n = 4$), M^{Mod} ($n = 7$) and M^{High} ($n = 6$) were comparable to those of L ($n = 4$) mice, indicating that delivery of CCL2/MCP-1 gene did not promote or suppress the growth of tumor cells in this model.

To determine whether CCL2/MCP-1 gene delivery can potentiate the antitumor effects of the HSV-tk/GCV system, mice were injected with BNL cells infected with rAds (Ad-tk, Ad-MCP1 and Ad-LacZ) at various MOIs as described in the Materials and methods. Whole livers were weighed on day 21, and the weights of T/M^{Low} ($n = 14$), T/M^{Mod} ($n = 12$), T/M^{High} ($n = 11$) and T/L ($n = 10$) mice were compared with those of N/L ($n = 10$) mice. The reduction in liver weight for the T/L mice was a result of the HSV-tk/GCV system alone, and those for T/M^{Low}, T/M^{Mod} and T/M^{High} were a result of treatment in combination with CCL2/MCP-1. Mean ± SEM liver weight was significantly lower in T/M^{Low} mice than in T/L mice (3.91 ± 0.36 g versus 5.80 ± 0.58 g; $p < 0.01$) (Figures 1D and 1E) as a result of the reduced growth of implanted tumor cells in the former. By contrast, the increase in liver weight was not suppressed in T/M^{Mod} and T/M^{High} mice whose tumor cells had been treated with higher titers of Ad-MCP1. Thus, only low level CCL2/MCP-1 provided additional antitumor effects and these results indicate that delivery of adequate amounts of Ad-MCP1 enhanced the antitumor effects of the HSV-tk/GCV system against intrahepatic tumor cells.

Serial analysis of liver histology following tumor cell transfer

To monitor the course of tumor development following HCC cell transfer, mouse livers were harvested on days 1, 3, 7 and 14. Livers harvested on day 1 from all groups of mice injected with BNL cells showed multiple white patches on their surfaces. Histologically, hepatocyte degeneration and necrosis were observed in these lesions, suggesting that the reduction of PV flow by transferred tumor cells induced focal ischemic necrosis in the livers (Figure 2, closed arrowheads). Although the extent of necrosis was similar among all groups, inflammatory cell infiltration in the area of necrosis was greater in T/M^{Low}, T/M^{High} and T/L than in N/L mice. On day 3, cellular infiltration disappeared, and tumor cell growth was observed in areas surrounding the necrotic regions. On day 7, proliferation of viable tumor cells surrounding the necrosis was seen in the livers of N/L mice, with the necrotic tissues completely replaced by tumor cells. Tumor growth was moderately inhibited in T/L mice and greatly inhibited in T/M^{Low} mice. There was no difference between T/L and T/M^{High} mice (not shown). On day 14, the necrotic areas were almost absorbed in all mice. In N/L mice, the tumor cells grew progressively and the tumor masses became larger. Tumor volume was relatively lower in T/L than in N/L mice, although there was no significant difference between T/L and T/M^{High} mice. The greatest degree of tumor growth inhibition was observed in T/M^{Low} mice (Figure 2).

Recruitment of immune cells in liver

To evaluate the involvement of immune responses in the CCL2/MCP-1 associated enhancement of the antitumor effects of rAd expressing HSV-tk, we assessed the recruitment of Mac-1^+ monocytes/macrophages and $CD4^+$ and $CD8^+$ T lymphocytes immunohistochemically (Figure 3).

T/M^{Low} and T/M^{High} mouse liver tissues harvested on day 1 showed marked infiltration of Mac-1^+ cells in the necrotic areas induced by tumor cell injection (Figure 3A). Quantitative morphometric analysis showed that the numbers of Mac-1^+ cells were significantly higher in liver tissues of T/M^{Low} and T/M^{High} mice [mean ± SEM of 40 high power (×400) fields of necrotic liver

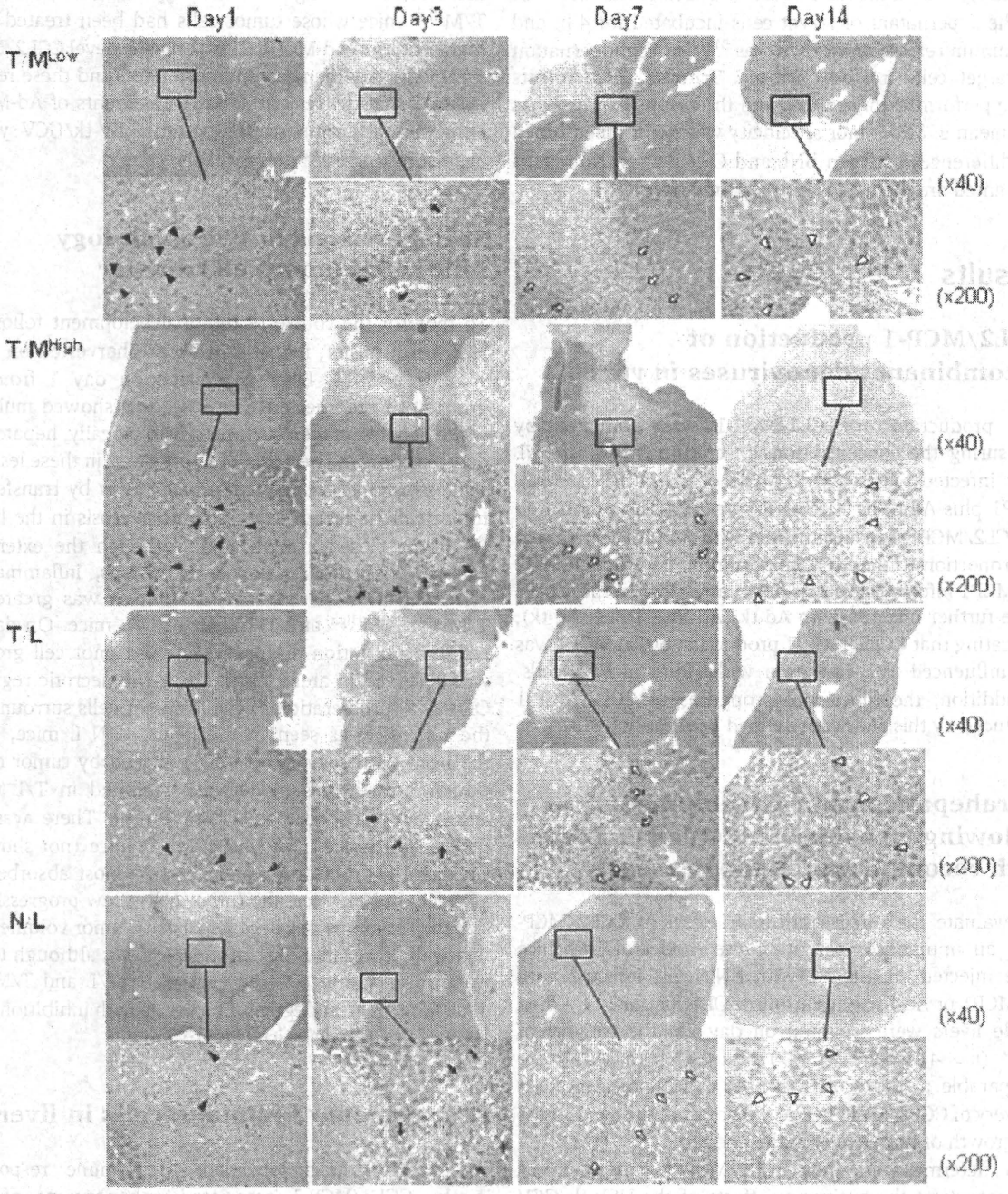

Figure 2. Serial analysis of liver histology following tumor cell transfer. Mouse liver tissues were harvested on days 1, 3, 7 and 14, and stained with H&E. On day 1, all mice injected with BNL cells showed multiple white patches on the liver surface (not shown). Histologically, hepatocyte degeneration and necrosis were observed in these lesions, suggesting that the reduction of PV flow by transferred tumor cells induced focal ischemic necrosis in the livers. The area of necrosis significantly infiltrated with inflammatory cells (closed arrowheads) was higher in T/M^{Low}, T/M^{High} and T/L mice than in N/L mice. On day 3, cellular infiltration disappeared and tumor cell growth (closed arrows) was detected in areas surrounding the necrotic regions. On day 7, tumor tissue enlarged and replaced the necrotic areas (open arrows). On day 14, the necrotic areas disappeared and tumor nodules eventually formed (open arrowheads). Original magnifications ×40 and ×200

J Gene Med 2010; 12: 1002–1013.
DOI: 10.1002/jgm

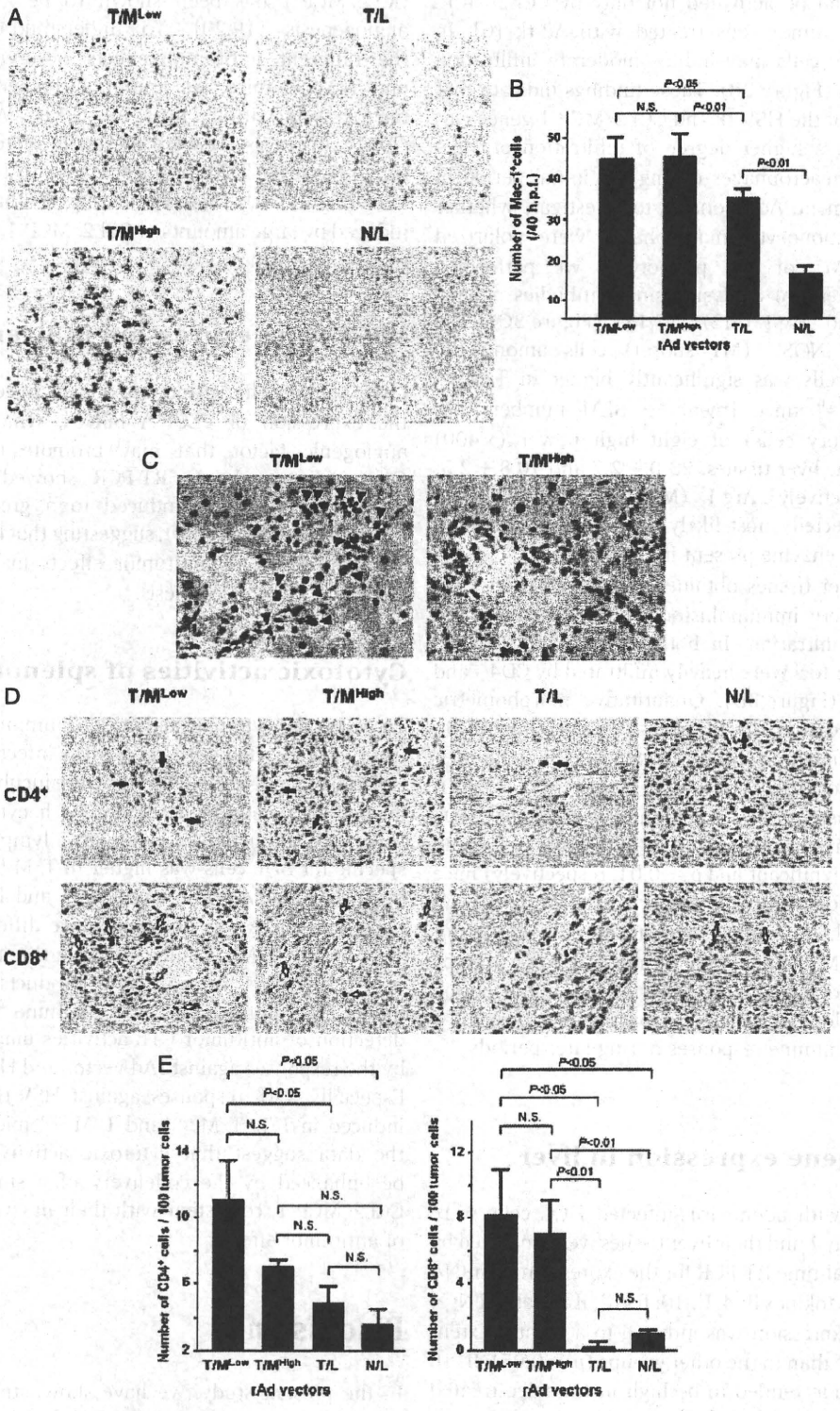

Figure 3. Immunohistochemical evaluation of monocyte/macrophage (A–C) and T cell (D, E) recruitment into liver tissues. (A) Monocyte/macrophage detection using anti-Mac-1 monoclonal antibody. Original magnification ×400. (B) Quantitative morphometric analysis of Mac-1$^+$ cells. (C) Immunohistochemical evaluation of the polarization towards M1 phenotype of recruited monocytes/macrophages using antibody against iNOS (closed arrowheads). (D) CD4$^+$ (closed arrows) and CD8$^+$ (open arrows) T cell detection. Original magnification ×400. (E) Quantitative morphometric analysis of CD4$^+$ and CD8$^+$ T cells

tissues: 46.5 ± 3.7 and 46.9 ± 3.7; $p < 0.05$ and $p < 0.01$, respectively] compared to T/L mice (35.2 ± 2.4). Macrophages can be activated not only by CCL2/MCP-1, but also by tumor cells treated with Ad-tk [6]. In T/L mice, these cells may induce moderate infiltration of Mac-1$^+$ cells (Figure 3B). These findings indicate that the codelivery of the HSV-tk and CCL2/MCP-1 genes was associated with a higher degree of infiltration of Mac-1$^+$ monocytes/macrophages during the initial period of tumor development. Additionally, to investigate whether the recruited monocytes/macrophages were polarized towards the M1 or M2 phenotype, we performed immunohistochemical analysis using antibodies against iNOS (M1) and Arg-I (M2) [17,18] (Figure 3C). The proportion of iNOS$^+$ (M1 subset) cells among the inflammatory cells was significantly higher in T/M^{Low} than in T/M^{High} mice [mean ± SEM number (per 100 inflammatory cells) of eight high power (×400) fields of necrotic liver tissues: 23.0 ± 2.7 and 10.8 ± 2.5; $p < 0.01$, respectively]. Arg-I$^+$ (M2 subset) cells were not specifically detected, most likely as a result of the large amounts of the enzyme present in liver tissues.

Similarly, liver tissues obtained on day 14 after HCC cell transfer were immunohistochemically analyzed for immune cell infiltration. In both T/M^{Low} and T/M^{High} mice, the tumor foci were heavily infiltrated by CD4$^+$ and CD8$^+$ T cells (Figure 3D). Quantitative morphometric analysis showed that the numbers of CD4$^+$ and CD8$^+$ T cells were higher in T/M^{Low} [mean ± SEM number (per 100 tumor cells) of eight high power (×400) fields of liver tissues: 11.1 ± 2.5 and 8.1 ± 2.7; $p < 0.05$ and $p < 0.05$, respectively] and T/M^{High} (7.1 ± 1.9 and 7.1 ± 0.7; not significant and $p < 0.01$, respectively) mice than in T/L mice (4.8 ± 1.1 and 0.3 ± 0.3, respectively) (Figure 3E). These results suggest that the antitumor activities in T/M^{Low} mice may be mediated not only by the activation of macrophages during the initial period of tumor development, but also by the induction of T cell mediated immune responses during later periods.

Cytokine gene expression in liver

Mice injected with adenovirus-infected HCC cells were sacrificed on day 1 and their liver tissues were analyzed by quantitative real-time RT-PCR for the expression of mRNA encoding the cytokines IL-4, IL-10, IL-12, IL-18 and IFN-γ. IL-12 mRNA expression was induced to a greater extent in T/M^{Low} mice than in the other groups ($p < 0.05$). IL-18 mRNA expression tended to be high in the mice treated with CCL2/MCP-1, although these differences were not statistically significant (Figure 4). By contrast, IL-4, IL-10 and IFN-γ mRNA was not detected in any samples. These data suggest that infiltrating monocytes/macrophages induced by CCL2/MCP-1 may be activated to enhance the Th1 polarized responses that contribute to tumor immunity.

Microvessels in HCC

CCL2/MCP-1 has been shown to be associated with angiogenesis [19,20]. To understand the basis of the different antitumor effects observed in T/M^{Low} and T/M^{High} mice, we immunohistochemically stained microvessels within HCCs for CD31. We found that CD31$^+$ microvessels were markedly increased in 7 day tumor tissues of T/M^{High} mice relative to T/M^{Low} and T/L mice (Figure 5A). These results suggest that angiogenesis induced by large amounts of CCL2/MCP-1 may contribute to tumor growth in T/M^{High} mice.

VEGF gene expression in liver

Liver samples harvested on day 3 were analyzed for the expression of VEGF-A mRNA, which encodes an angiogenic factor that may promote tumor growth. Quantitative real-time RT-PCR showed that VEGF-A gene expression was induced to a greater extent in T/M^{High} mice (Figure 5B), suggesting that the CCL2/MCP-1 enhancement of antitumor effects may be offset by VEGF-induced angiogenesis.

Cytotoxic activities of splenocytes

To assess the cytotoxic activities of immune cells derived from mice injected with adenovirus-infected tumor cells, isolated and pulsed splenocytes were incubated with ^{51}Cr-labeled BNL cells in a standard 4-h cytotoxicity assay (Figure 6). Induction of cytotoxic T lymphocytes (CTLs) specific for BNL cells was higher in T/M^{Low} and T/M^{High} mice than in T/L (not significant) and N/L ($p < 0.01$) mice, and there was no significance difference between T/M^{Low} and T/M^{High} mice. Because the immunogenicity of viral vectors or transgene products is known to induce the unfavorable host immune responses, the detection of antitumor CTL activities may be influenced by the responses against rAd vector and HSV-tk [21-23]. Especially, CTL responses against HSV-tk appear to be induced in T/L, T/M^{Low} and T/M^{High} mice. Collectively, the data suggest that cytotoxic activity of CTLs may be enhanced by the codelivery of a suicide gene and CCL2/MCP-1, consistent with their *in vivo* enhancement of antitumor effects.

Discussion

In the present study, we have shown that combination gene therapy, using the HSV-tk/GCV system and CCL2/MCP-1 gene delivery, was effective for the treatment of HCC in a mouse model of IM. Delivery of an adequate amount of CCL2/MCP-1 enhanced the antitumor effects of the HSV-tk/GCV system against intrahepatic tumor cells. Necrotic areas induced by HCC tumor cell injection showed marked infiltration of iNOS

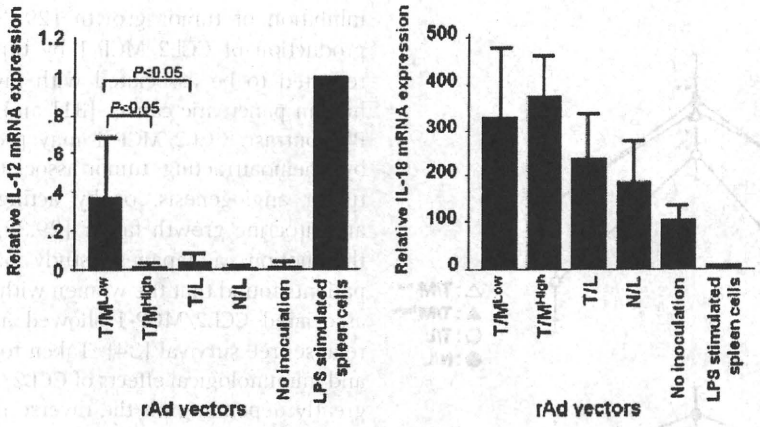

Figure 4. Real-time quantitative RT-PCR for IL-12 and IL-18 mRNA expression in the liver on day 1. IL-12 gene expression was significantly higher in T/M^{Low} mice than in the other groups ($p < 0.05$)

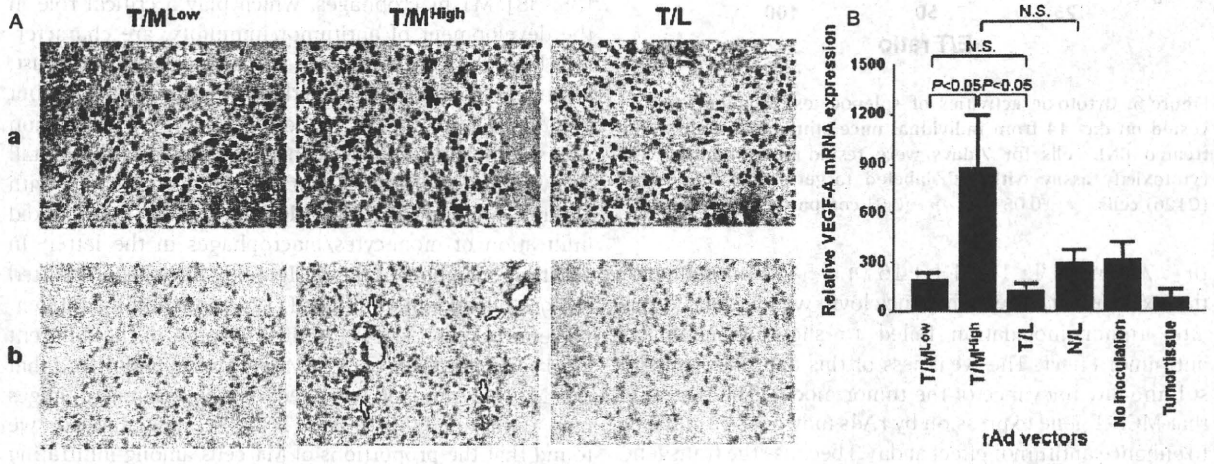

Figure 5. Evaluation of tumor angiogenesis. (A) Morphometric analysis of microvessels in tumor tissues using H&E staining and CD31 immunohistochemical analysis. (a) Representative H&E stained histological sections of day 7 tumor tissues showing intratumoral microvessels containing red blood cells (closed arrow); endothelial cells were not identified. (b) Representative CD31 immunohistochemical staining showing endothelial cell proliferation in tumor tissues (open arrow). Original magnification ×400. (B) Real-time quantitative RT-PCR for VEGF-A mRNA expression in liver on day 3

monocytes/macrophages and IL-12 production on day 1, and the tumor foci showed heavy infiltration by $CD4^+$ and $CD8^+$ T cells on day 14. CTLs specific for BNL cells were induced in mice treated with CCL2/MCP-1. By contrast, the expression of the angiogenic factor VEGF-A was significantly increased in mice treated with a large amount of CCL2/MCP-1. Collectively, these results suggest that the delivery of an adequate amount of CCL2/MCP-1, in conjunction with the HSV-tk/GCV system, may display beneficial antitumor effects, preventing the intrahepatic metastasis of HCC cells.

In the development of this model, we injected 1×10^6 tumor cells infected with recombinant adenoviruses into the portal vein because the injection of fewer cells (e.g. 10^5) resulted in greatly diminished frequencies of metastasis in the mice. The injection of large numbers of cells, however, may have caused the embolization of cell aggregates in the portal vein, which may have contributed to the induction of ischemic necrosis in the liver tissues. The resultant ischemic death of liver cells may be recognized by immune cells including macrophages, and may result in macrophage activation and the local release of cytokines and chemokines. However, when the mice were injected with control tumor cells (N/L), we observed little infiltration of immune cells, including macrophages and $CD4^+$ and $CD8^+$ T cells, and these mice developed the largest amounts of tumor tissues. These results indicate that any unfavorable effects as a result of ischemic cell death were minimal for the development of intrahepatic metastasis in this model.

This model would be more relevant if ganciclovir treatment was delayed to allow the establishment of tumors. Therefore, we performed the additional experiments with ganciclovir treatment at delayed time point, day 3. Although there was a trend for small amount of MCP-1 to enhance the antitumor effects of the HSV-tk/GCV system, as seen in the experiments on day 1, these differences did not reach statistical significance [T/M^{Low}: 7.64 ± 1.25 ($n = 10$); T/M^{Mod}: 9.24 ± 0.77 ($n = 5$); T/M^{High}: 9.65 ± 1.06 ($n = 8$); T/L: 10.51 ± 1.79

DOI: 10.1002/jgm

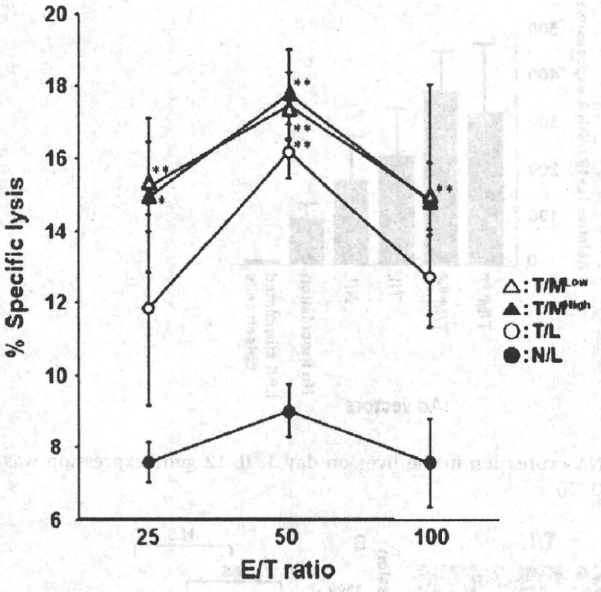

Figure 6. Cytotoxic activities of splenocytes. Splenocytes harvested on day 14 from individual mice stimulated with MMC-treated BNL cells for 7 days were tested in a standard 4-h cytotoxicity assay with ^{51}Cr-labeled target (BNL) or control (CT26) cells. $^{*}p < 0.05$ and $^{**}p < 0.01$ compared to N/L mice

($n = 7$); and N/L: 13.94 ± 1.16 ($n = 5$)]. Consequently, the experiment in which ganciclovir was added 3 days after tumor inoculation failed to show a significant antitumor effect. The weakness of this approach may be still the low relevance of the tumor model. The reason is that MCP-1 gene expression by rAds may not be sufficient to enhance antitumor effect at day 3 because the transgene expression gradually diminished with the tumor growth. In our previous studies, MCP-1 production reached peak level on day 2 and decreased after day 3 [6].

Mice treated with small amounts of CCL2/MCP-1 showed enhancement of antitumor effects. The amount of CCL2/MCP-1 delivered, however, was not correlated with monocyte/macrophage accumulation. Although activated monocytes/macrophages are indicative of the potential to eliminate tumor cells [24–26], infiltrating macrophages may enhance tumor growth by secreting growth and angiogenic factors, including VEGF [26–28]. Immunohistochemical analysis of CD31 revealed that microvessels in HCCs were increased in the mice treated with large amounts of CCL2/MCP-1. We also observed a close correlation between the amounts of CCL2/MCP-1 delivered and the levels of VEGF expression. These findings suggest that large amounts of CCL2/MCP-1 may recruit macrophages to induce tumor cell killing and, simultaneously, to facilitate tumor growth, probably by promoting angiogenesis, thus resulting in a reduction of antitumor effects.

CCL2/MCP-1 is a member of the CC chemokine superfamily that promotes the migration of macrophages/monocytes, T lymphocytes, natural killer cells and natural killer T cells not only to sites of inflammation, but also to tumor tissues, which may contribute to the inhibition of tumor growth [29–31]. In addition, the production of CCL2/MCP-1 by tumor tissues has been reported to be associated with favorable prognoses in human pancreatic cancer [31] and neuroblastoma [30]. By contrast, CCL2/MCP-1 may promote tumor growth by chemoattracting tumor-associated macrophages for tumor angiogenesis, or by acting on tumor cells as an autocrine growth factor [29,32,33]. Consistent with this notion, a Japanese study of 135 breast cancer patients found that the women with high levels of tumor-associated CCL2/MCP-1 showed a significantly shorter relapse-free survival [34]. Taken together, the biological and immunological effects of CCL2/MCP-1 appear to vary greatly depending on the diverse microenvironments of cancer tissues.

Two major types of activated macrophages have been described: M1 (classical) and M2 (alternative) [35–38]. M1 macrophages, which play a critical role in the development of antitumor immunity, are characterized by high IL-12 and low IL-10 production. By contrast, M2 macrophages produce reduced amounts of IL-12 but higher levels of Il–10. We found that IL-12 expression was significantly increased in mice treated with a small amount of CCL2/MCP-1 but not in mice treated with a large amount of CCL2/MCP-1, despite the marked infiltration of monocytes/macrophages in the latter. In addition, members of the MCP family have been reported to dose-dependently inhibit IL-12 production by antigen presenting cells (APCs) [39,40]. Because of the different local concentrations of CCL/MCP-1, we hypothesized that the M1/M2 ratio of recruited monocytes/macrophages may differ in T/M^{Low} and T/M^{High} mice. Indeed, we found that the proportions of M1 cells among infiltrating cells were significantly higher in T/M^{Low} than in T/M^{High} mice. Therefore, M1 monocyte/macrophage polarization may be suppressed in mice treated with large amounts of CCL2/MCP-1, resulting in the reduction of antitumor immunity and the promotion of tumor growth.

Significant tumor infiltration of CD4$^+$ and CD8$^+$ T cells 14 days after transfer was observed in mice treated with the HSV-tk/GCV system plus CCL2/MCP-1. Local secretion of CCL2/MCP-1 by tumor cells may lead to the recruitment and activation of antigen-presenting monocytes/macrophages [41,42]. Once attracted to the tumor tissues, these APCs may ingest pathogenic antigens and transport them to local lymphoid organs, where the antigens are presented to naive T cells, thus establishing a T cell-mediated antitumor response [43]. Tumor growth may thus be impeded by tumor antigen-specific CD4$^+$ and CD8$^+$ T cells.

Although the data obtained in the present study appear to be promising, several problems remain to be solved before clinical application. Our liver metastasis model using a mouse HCC cell line may not be comparable to intrahepatic metastasis of HCC in human patients. However, HCC patients treated by nonsurgical procedures, including percutaneous radiofrequency ablation therapy and transcatheter arterial chemotherapy [44,45], could also be administered rAds to reduce the incidence of

intrahepatic recurrence and metastasis. The present study demonstrated that, in a mouse model, there is a negative impact on tumor development in the presence of a low level of CCL2/MCP-1, whereas high levels of the protein complicate the situation by having a positive impact on tumor growth (i.e. a balance is required). The therapeutic effects may vary with different tumors. The direct correlation between the overexpression of VEGF in tumor cells and tumor angiogenesis has been demonstrated previously [46], and large amount of CCL2/MCP-1 might be less effective in the treatment of hypervascular tumors such as HCC. However, other cancers resistant to anti-angiogenic drug (e.g. pancreatic cancer) [47,48], probably do not need a good blood supply for tumor growth. In the treatment of hypovascular tumors that are resistant to anti-angiogenic drug, CCL2/MCP-1 may enhance the antitumor effects via activation of M1 macrophages.

Additionally, in the present study, we did not perform *in vivo* delivery experiments of the vectors to existing tumors. There would be many complicated factors affecting the delivery of HSV-tk and CCL2/MCP-1 genes in therapeutic approaches [49,50]. Intra-arterial administration of rAds may result in the induction of immunogenicity or cytotoxicity, especially when spread via blood flow. Extremely high-dose rAds have been found to cause severe unexpected side-effects [51]. To overcome these problems, highly tumor-specific promoters may be needed. In our previous studies, human alpha-fetoprotein (AFP) promoters specific for liver cancer cells were used in an immunodeficient nude mouse models [6,52]. A reporter gene was specifically expressed in AFP producing tumors that were xenografted subcutaneously and disseminated in the liver and lung. However, HSV-tk gene expression was not enhanced sufficiently to kill established tumor cells [53] because the transcriptional activity of AFP promoter was relatively low. Furthermore, neither promoters, nor delivery systems were found to be specific for the BNL mouse tumor cell line. Although better methods of tumor-specific gene delivery and expression are needed, the use of *ex vivo* infection techniques has been found to reproduce tumor specific gene expression *in vivo*.

Conclusions

Although problems with rAds remain to be resolved before clinical application, the results obtained in the present study suggest that a new strategy, consisting of immune gene therapy accompanied by a suicide gene system, can be used to treat HCC and tumors of other lineages.

Acknowledgements

We thank Akemi Nakano, Yuzu Hasebe and Yui Fujita for their assistance with the histopathological analysis and immunohistochemistry. We are also grateful to Maki Kawamura and Chiharu Minami for providing animal care.

References

1. Llovet JM, Burroughs A, Bruix J. Hepatocellular carcinoma. *Lancet* 2003; **362:** 1907–1917.
2. Izumi N, Asahina Y, Noguchi O, *et al.* Risk factors for distant recurrence of hepatocellular carcinoma in the liver after complete coagulation by microwave or radiofrequency ablation. *Cancer* 2001; **91:** 949–956.
3. Poon RT, Fan ST, Ng IO, Lo CM, Liu CL, Wong J. Different risk factors and prognosis for early and late intrahepatic recurrence after resection of hepatocellular carcinoma. *Cancer* 2000; **89:** 500–507.
4. Arii S, Monden K, Niwano M, *et al.* Results of surgical treatment for recurrent hepatocellular carcinoma; comparison of outcome among patients with multicentric carcinogenesis, intrahepatic metastasis, and extrahepatic recurrence. *J Hepatobil Pancreat Surg* 1998; **5:** 86–92.
5. Miyata R, Tanimoto A, Wakabayashi G, *et al.* Accuracy of preoperative prediction of microinvasion of portal vein in hepatocellular carcinoma using superparamagnetic iron oxide-enhanced magnetic resonance imaging and computed tomography during hepatic angiography. *J Gastroenterol* 2006; **41:** 987–995.
6. Sakai Y, Kaneko S, Nakamoto Y, Kagaya T, Mukaida N, Kobayashi K. Enhanced anti-tumor effects of herpes simplex virus thymidine kinase/ganciclovir system by code-livering monocyte chemoattractant protein-1 in hepatocellular carcinoma. *Cancer Gene Ther* 2001; **8:** 695–704.
7. Tsuchiyama T, Kaneko S, Nakamoto Y, *et al.* Enhanced antitumor effects of a bicistronic adenovirus vector expressing both herpes simplex virus thymidine kinase and monocyte chemoattractant protein-1 against hepatocellular carcinoma. *Cancer Gene Ther* 2003; **10:** 260–269.
8. Tsuchiyama T, Nakamoto Y, Sakai Y, *et al.* Prolonged, NK cell-mediated antitumor effects of suicide gene therapy combined with monocyte chemoattractant protein-1 against hepatocellular carcinoma. *J Immunol* 2007; **178:** 574–583.
9. Rollins BJ, Sunday ME. Suppression of tumor formation in vivo by expression of the JE gene in malignant cells. *Mol Cell Biol* 1991; **11:** 3125–3131.
10. Hirose K, Hakozaki M, Nyunoya Y, *et al.* Chemokine gene transfection into tumour cells reduced tumorigenicity in nude mice in association with neutrophilic infiltration. *Br J Cancer* 1995; **72:** 708–714.
11. Huang S, Singh RK, Xie K, *et al.* Expression of the JE/MCP-1 gene suppresses metastatic potential in murine colon carcinoma cells. *Cancer Immunol Immunother* 1994; **39:** 231–238.
12. Kanegae Y, Lee G, Sato Y, *et al.* Efficient gene activation in mammalian cells by using recombinant adenovirus expressing site-specific Cre recombinase. *Nucleic Acids Res* 1995; **23:** 3816–3821.
13. Miyake S, Makimura M, Kanegae Y, *et al.* Efficient generation of recombinant adenoviruses using adenovirus DNA-terminal protein complex and a cosmid bearing the full-length virus genome. *Proc Natl Acad Sci USA* 1996; **93:** 1320–1324.
14. Sato Y, Tanaka K, Lee G, *et al.* Enhanced and specific gene expression via tissue-specific production of Cre recombinase using adenovirus vector. *Biochem Biophys Res Commun* 1998; **244:** 455–462.

15. Matthews DA, Russell WC. Adenovirus protein–protein interactions: hexon and protein VI. *J Gen Virol* 1994; **75:** 3365–3374.
16. Kanegae Y, Makimura M, Saito I. A simple and efficient method for purification of infectious recombinant adenovirus. *Jpn J Med Sci Biol* 1994; **47:** 157–166.
17. Benoit M, Desnues B, Mege JL. Macrophage polarization in bacterial infections. *J Immunol* 2008; **181:** 3733–3739.
18. Redente EF, Orlicky DJ, Bouchard RJ, Malkinson AM. Tumor signaling to the bone marrow changes the phenotype of monocytes and pulmonary macrophages during urethane-induced primary lung tumorigenesis in A/J mice. *Am J Pathol* 2007; **170:** 693–708.
19. Salcedo R, Ponce ML, Young HA, *et al.* Human endothelial cells express CCR2 and respond to MCP-1: direct role of MCP-1 in angiogenesis and tumor progression. *Blood* 2000; **96:** 34–40.
20. Koga M, Kai H, Egami K, *et al.* Mutant MCP-1 therapy inhibits tumor angiogenesis and growth of malignant melanoma in mice. *Biochem Biophys Res Commun* 2008; **365:** 279–284.
21. Berger C, Flowers ME, Warren EH, Riddell SR. Analysis of transgene-specific immune responses that limit the in vivo persistence of adoptively transferred HSV-TK-modified donor T cells after allogeneic hematopoietic cell transplantation. *Blood* 2006; **107:** 2294–2302.
22. Raty JK, Lesch HP, Wirth T, Yla-Herttuala S. Improving safety of gene therapy. *Curr Drug Safety* 2008; **3:** 46–53.
23. Schagen FH, Ossevoort M, Toes RE, Hoeben RC. Immune responses against adenoviral vectors and their transgene products: a review of strategies for evasion. *Crit Rev Oncol Hematol* 2004; **50:** 51–70.
24. Bonta IL, Ben-Efraim S. Involvement of inflammatory mediators in macrophage antitumor activity. *J Leukoc Biol* 1993; **54:** 613–626.
25. Hock H, Dorsch M, Kunzendorf U, Qin Z, Diamantstein T, Blankenstein T. Mechanisms of rejection induced by tumor cell-targeted gene transfer of interleukin 2, interleukin 4, interleukin 7, tumor necrosis factor, or interferon gamma. *Proc Natl Acad Sci USA* 1993; **90:** 2774–2778.
26. Mantovani A, Bottazzi B, Colotta F, Sozzani S, Ruco L. The origin and function of tumor-associated macrophages. *Immunol Today* 1992; **13:** 265–270.
27. Leung SY, Wong MP, Chung LP, Chan AS, Yuen ST. Monocyte chemoattractant protein-1 expression and macrophage infiltration in gliomas. *Acta Neuropathol (Berl)* 1997; **93:** 518–527.
28. Sunderkotter C, Steinbrink K, Goebeler M, Bhardwaj R, Sorg C. Macrophages and angiogenesis. *J Leukoc Biol* 1994; **55:** 410–422.
29. Conti I, Rollins BJ. CCL2 (monocyte chemoattractant protein-1) and cancer. *Semin Cancer Biol* 2004; **14:** 149–154.
30. Raffaghello L, Cocco C, Corrias MV, Airoldi I, Pistoia V. Chemokines in neuroectodermal tumour progression and metastasis. *Semin Cancer Biol* 2009; **19:** 97–102.
31. Monti P, Leone BE, Marchesi F, *et al.* The CC chemokine MCP-1/CCL2 in pancreatic cancer progression: regulation of expression and potential mechanisms of antimalignant activity. *Cancer Res* 2003; **63:** 7451–7461.
32. Loberg RD, Ying C, Craig M, Yan L, Snyder LA, Pienta KJ. CCL2 as an important mediator of prostate cancer growth in vivo through the regulation of macrophage infiltration. *Neoplasia (New York)* 2007; **9:** 556–562.
33. Porta C, Subhra Kumar B, Larghi P, Rubino L, Mancino A, Sica A. Tumor promotion by tumor-associated macrophages. *Adv Exp Med Biol* 2007; **604:** 67–86.
34. Ueno T, Toi M, Saji H, *et al.* Significance of macrophage chemoattractant protein-1 in macrophage recruitment, angiogenesis, and survival in human breast cancer. *Clin Cancer Res* 2000; **6:** 3282–3289.
35. Mosser DM. The many faces of macrophage activation. *J Leukoc Biol* 2003; **73:** 209–212.
36. Edwards JP, Zhang X, Frauwirth KA, Mosser DM. Biochemical and functional characterization of three activated macrophage populations. *J Leukoc Biol* 2006; **80:** 1298–1307.
37. Mantovani A, Sica A, Sozzani S, Allavena P, Vecchi A, Locati M. The chemokine system in diverse forms of macrophage activation and polarization. *Trends Immunol* 2004; **25:** 677–66.
38. Gratchev A, Kzhyshkowska J, Kothe K, *et al.* Mphi1 and Mphi2 can be re-polarized by Th2 or Th1 cytokines, respectively, and respond to exogenous danger signals. *Immunobiology* 2006; **211:** 473–486.
39. Braun MC, Lahey E, Kelsall BL. Selective suppression of IL-12 production by chemoattractants. *J Immunol* 2000; **164:** 3009–3017.
40. Matsunaga K, Klein TW, Newton C, Friedman H, Yamamoto Y. Legionella pneumophila suppresses interleukin-12 production by macrophages. *Infect Immun* 2001; **69:** 1929–1933.
41. Gu L, Tseng S, Horner RM, Tam C, Loda M, Rollins BJ. Control of TH2 polarization by the chemokine monocyte chemoattractant protein-1. *Nature* 2000; **404:** 407–411.
42. Carr MW, Roth SJ, Luther E, Rose SS, Springer TA. Monocyte chemoattractant protein 1 acts as a T-lymphocyte chemoattractant. *Proc Natl Acad Sci USA* 1994; **91:** 3652–3656.
43. Baggiolini M, Dewald B, Moser B. Human chemokines: an update. *Annu Rev Immunol* 1997; **15:** 675–705.
44. Curley SA. Radiofrequency ablation of malignant liver tumors. *Ann Surg Oncol* 2003; **10:** 338–347.
45. Tung-Ping Poon R, Fan ST, Wong J. Risk factors, prevention, and management of postoperative recurrence after resection of hepatocellular carcinoma. *Ann Surg* 2000; **232:** 10–24.
46. Mise M, Arii S, Higashituji H, *et al.* Clinical significance of vascular endothelial growth factor and basic fibroblast growth factor gene expression in liver tumor. *Hepatology (Baltimore)* 1996; **23:** 455–464.
47. Kindler HL, Niedzwiecki D, Hollis D, *et al.* Gemcitabine plus bevacizumab compared with gemcitabine plus placebo in patients with advanced pancreatic cancer: phase III trial of the Cancer and Leukemia Group B (CALGB 80303). *J Clin Oncol* 2010; **28:** 3617–3622.
48. Philip PA, Benedetti J, Corless CL, *et al.* Phase III study comparing gemcitabine plus cetuximab versus gemcitabine in patients with advanced pancreatic adenocarcinoma: Southwest Oncology Group-directed intergroup trial S0205. *J Clin Oncol* 2010; **28:** 3605–3610.
49. Cassidy J, Schatzlein AG. Tumour-targeted drug and gene delivery: principles and concepts. *Exp Reviews Mol Med* 2004; **6:** 1–17.
50. Yu P, Wang X, Fu YX. Enhanced local delivery with reduced systemic toxicity: delivery, delivery, and delivery. *Gene Ther* 2006; **13:** 1131–1132.
51. Marshall E. Gene therapy death prompts review of adenovirus vector. *Science* 1999; **286:** 2244–2245.
52. Kaneko S, Hallenbeck P, Kotani T, *et al.* Adenovirus-mediated gene therapy of hepatocellular carcinoma using cancer-specific gene expression. *Cancer Res* 1995; **55:** 5283–5287.
53. Sakai Y, Kaneko S, Sato Y, *et al.* Gene therapy for hepatocellular carcinoma using two recombinant adenovirus vectors with alpha-fetoprotein promoter and Cre/lox P system. *J Virol Methods* 2001; **92:** 5–17.

Published OnlineFirst May 18, 2010; DOI:10.1158/0008-5472.CAN-09-4210

Tumor and Stem Cell Biology

Cancer Research

Oncostatin M Renders Epithelial Cell Adhesion Molecule–Positive Liver Cancer Stem Cells Sensitive to 5-Fluorouracil by Inducing Hepatocytic Differentiation

Taro Yamashita, Masao Honda, Kouki Nio, Yasunari Nakamoto, Tatsuya Yamashita, Hiroyuki Takamura, Takashi Tani, Yoh Zen, and Shuichi Kaneko

Abstract

Recent evidence suggests that a certain type of hepatocellular carcinoma (HCC) is hierarchically organized by a subset of cells with stem cell features (cancer stem cells; CSC). Although normal stem cells and CSCs are considered to share similar self-renewal programs, it remains unclear whether differentiation programs are also maintained in CSCs and effectively used for tumor eradication. In this study, we investigated the effect of oncostatin M (OSM), an interleukin 6–related cytokine known to induce the differentiation of hepatoblasts into hepatocytes, on liver CSCs. OSM receptor expression was detected in the majority of epithelial cell adhesion molecule–positive ($EpCAM^+$) HCC with stem/progenitor cell features. OSM treatment resulted in the induction of hepatocytic differentiation of $EpCAM^+$ HCC cells by inducing signal transducer and activator of transcription 3 activation, as determined by a decrease in stemness-related gene expression, a decrease in EpCAM, α-fetoprotein and cytokeratin 19 protein expressions, and an increase in albumin protein expression. OSM-treated $EpCAM^+$ HCC cells showed enhanced cell proliferation with expansion of the EpCAM-negative non-CSC population. Noticeably, combination of OSM treatment with the chemotherapeutic agent 5-fluorouracil (5-FU), which eradicates EpCAM-negative non-CSCs, dramatically increased the number of apoptotic cells *in vitro* and suppressed tumor growth *in vivo* compared with either saline control, OSM, or 5-FU treatment alone. Taken together, our data suggest that OSM could be effectively used for the differentiation and active cell division of dormant $EpCAM^+$ liver CSCs, and the combination of OSM and conventional chemotherapy with 5-FU efficiently eliminates HCC by targeting both CSCs and non-CSCs. *Cancer Res; 70(11); 4687–97. ©2010 AACR.*

Introduction

It is widely accepted that cancer is a disease that develops from a normal cell with accumulated genetic/epigenetic changes. Although considered monoclonal in origin, cancer is composed of heterogeneous cellular populations. These heterogeneities are traditionally explained by the clonal evolution of cancer cells through a series of stochastic genetic events (clonal evolution model; ref. 1). In contrast, cancer cells are known to have the capabilities characteristic of stem cells with respect to self-renewal, limitless division, and generation of heterogeneous cell populations. Recent evidence suggests that tumor cells possess stem cell features (cancer stem cells; CSC) to self-renew and give rise to relatively differentiated cells through asymmetric division, and thereby form heterogeneous populations (CSC model; refs. 2, 3). Accumulating evidence supports the notion that CSCs could generate tumors more efficiently in immunodeficient mice than non-CSCs in the case of leukemia and various solid tumors (4–9), although the origin of CSCs is still a controversial issue.

Worldwide, hepatocellular carcinoma (HCC) is one of the most common malignancies with poor outcome (10). Recent evidence suggests that at least some HCCs are organized by liver CSCs in a hierarchical manner (11). Several markers have been identified as useful for the enrichment of liver CSCs, including side population fraction (12), CD133 (13), CD90 (14), and OV6 (15). We have recently used epithelial cell adhesion molecule (EpCAM) and α-fetoprotein (AFP) to identify novel prognostic HCC subtypes related to certain developmental stages of human liver lineages (16). Among these, EpCAM-positive ($^+$) AFP^+ HCC (hepatic stem cell–like HCC) is characterized by young onset of disease, activation of Wnt/β-catenin signaling, and poor prognosis. *EPCAM* is a target gene of Wnt/β-catenin signaling (17), and we previously identified that $EpCAM^+$ HCC cells from primary HCC

Authors' Affiliation: Center for Liver Diseases, Kanazawa University Hospital, Kanazawa, Ishikawa, Japan

Note: Supplementary data for this article are available at Cancer Research Online (http://cancerres.aacrjournals.org/).

Corresponding Authors: Taro Yamashita, Department of Gastroenterology, Kanazawa University Graduate School of Medical Science, 13-1 Takara-Machi, Kanazawa, Ishikawa 920-8641, Japan. Phone: 81-76-265-2851; Fax: 81-76-265-4250; E-mail: taroy@m-kanazawa.jp and Shuichi Kaneko, Center for Liver Diseases, Kanazawa University Hospital; Department of Gastroenterology, Kanazawa University Graduate School of Medical Science, 13-1 Takara-Machi, Kanazawa, Ishikawa 920-8641, Japan. Phone: 81-76-265-2230; Fax: 81-76-265-4250; E-mail: skaneko@m-kanazawa.jp.

doi: 10.1158/0008-5472.CAN-09-4210

Published OnlineFirst May 18, 2010; DOI:10.1158/0008-5472.CAN-09-4210

samples and cell lines have the features of CSCs, at least in the hepatic stem cell–like HCC subtype (18). Thus, EpCAM seems to be a potentially useful marker for the isolation of liver CSCs in hepatic stem cell–like HCC.

CSCs are considered to be resistant to chemotherapy and radiotherapy (19–21), which may be associated with the recurrence of the tumor after treatment. These findings have led to the proposal of "destemming" CSCs, to induce the differentiation of CSCs into non-CSCs or to eradicate CSCs by inhibiting the signaling pathway responsible for self-renewal (22). Recent studies support this proposal and suggest the utility of bone morphogenetic proteins, activated during embryogenesis and required for differentiation of neuronal stem cells, to induce differentiation of brain CSCs and facilitate brain tumor eradication (23, 24). However, it is still debatable whether simple differentiation of CSCs effectively eradicates tumors (25).

Oncostatin M (OSM), an interleukin (IL)-6–related cytokine produced by $CD45^+$ hematopoietic cells, is known to enhance hepatocytic differentiation of hepatoblasts by inducing the activation of the signal transducer and activator of transcription 3 (STAT3) pathway (26). Although OSM, IL-6, and leukemia-inhibitory factor share STAT3 signaling cascades, OSM is known to exploit the distinct hepatocytic differentiation signaling in an OSM receptor (OSMR)–specific manner (27). In this study, we hypothesized that OSM induces hepatocytic differentiation of liver CSCs through the OSMR signaling pathway. We examined OSMR expression and the effect of OSM in $EpCAM^+$ HCC in terms of hepatocytic differentiation and antitumor activities.

Materials and Methods

Clinical HCC specimens

A total of 107 HCC tissues and adjacent noncancerous liver tissues were obtained from patients who underwent hepatectomy for HCC treatment from 1999 to 2007 in Kanazawa University Hospital. These samples were formalin-fixed and paraffin-embedded, and used for immunohistochemistry. HCC and adjacent noncancerous liver tissues were histologically diagnosed by two pathologists. An additional fresh $EpCAM^+$ AFP^+ HCC sample was obtained from a surgically resected specimen and immediately used for the preparation of single-cell suspensions and xenotransplantation. All tissue acquisition procedures were approved by the Ethics Committee and the Institutional Review Board of Kanazawa University Hospital. All patients provided written informed consent.

Cell culture and reagents

HuH1 and HuH7 cells were cultured as previously described (18). A primary HCC tissue was dissected and digested in 1 μg/mL of type 4 collagenase (Sigma-Aldrich Japan K.K.) solution at 37°C for 15 to 30 minutes. Contaminated RBC were lysed with ammonium chloride solution (STEMCELL Technologies) on ice for 5 minutes. $CD45^+$ leukocytes and Annexin V^+ apoptotic cells were removed by autoMACS-pro cell separator and magnet beads (Miltenyi Biotec K.K.). EpCAM-positive and -negative cells were enriched by autoMACS-pro cell separator and CD326 (EpCAM) MicroBeads (Miltenyi Biotec K.K.). Recombinant OSM was purchased from R&D Systems, Inc. 5-Fluorouracil (5-FU) was obtained from Kyowa Kirin.

Quantitative reverse transcription-PCR analysis

Total RNA was extracted using TRIzol (Invitrogen) according to the instructions of the manufacturer. The expression of selected genes was determined in triplicate using the 7900 Sequence Detection System (Applied Biosystems). Each sample was normalized relative to β-actin expression. Probes used were *TACSTD1*, Hs00158980_m1; *AFP*, Hs00173490_m1; *KRT19*, Hs00761767_s1; *hTERT*, Hs00162669_m1; *Bmi1*, Hs00180411_m1; *POU5F1*, Hs00999632_g1; *CYP3A4*, Hs00430021_m1; *OSMR*, Hs00384278_m1; and *ACTB*, Hs99999903_m1 (Applied Biosystems).

Western blotting

Whole cell lysates were prepared using radioimmunoprecipitation assay lysis buffer as described previously (28). Rabbit polyclonal antibodies to STAT3 (Cell Signaling Technology, Inc.), rabbit polyclonal anti-OSMR antibodies H-200 (Santa Cruz Biotechnology), mouse monoclonal anti–phosphorylated STAT3 (Tyr^{705}) antibody (3E2; Cell Signaling Technology), and mouse monoclonal anti–β-actin antibody (Sigma-Aldrich) were used. Immune complexes were visualized by enhanced chemiluminescence (Amersham Biosciences, Corp.) as described by the manufacturer.

Immunohistochemistry and immunofluorescence analyses

Immunohistochemistry was performed using Envision+ kits (DAKO) according to the instructions of the manufacturer. Anti-EpCAM monoclonal antibody, VU-1D9 (Oncogene Research Products), was used for detecting EpCAM. Goat anti-OSMR polyclonal antibodies (C-20) were obtained from Santa Cruz Biotechnology. Mouse anti-CYP3A4 polyclonal antibodies (Abnova), mouse anti–cytokeratin (CK) 19 monoclonal antibody (DAKO), and mouse anti–Ki-67 monoclonal antibody MIB-1 (DAKO) were used for detecting CYP3A4, CK19, and Ki-67, respectively. Samples with >5% positive staining in a given area for a particular antibody were considered to be positive. For immunofluorescence analyses, anti-EpCAM antibody (Oncogene Research Products), anti-gp130ST antibodies (Santa Cruz Biotechnology), and anti–phosphorylated STAT3 (Tyr^{705}) antibody (3E2; Cell Signaling Technology) were used. Alexa 488 FITC-conjugated anti-mouse IgG or Alexa 568 Texas red–conjugated anti-goat/rabbit IgG (Molecular Probes) were used as secondary antibodies. Confocal fluorescence microscopic analysis was performed essentially as previously described (18).

Fluorescence-activated cell sorting analyses

Cultured cells were trypsinized, washed, and resuspended in HBSS (Lonza) supplemented with 1% HEPES and 2% fetal bovine serum (FBS). Cells were then incubated with FITC-conjugated anti-EpCAM monoclonal antibody Clone Ber-EP4 (DAKO) on ice for 30 minutes, and analyzed using

Published OnlineFirst May 18, 2010; DOI:10.1158/0008-5472.CAN-09-4210

a FACSCalibur (BD Biosciences). Intracellular AFP, CK19, and albumin levels were examined using a BD Cytofix/Cytoperm Fixation/Permeabilization Kit (BD Biosciences), anti-AFP mouse monoclonal antibody (Nichirei Biosciences Inc.), anti-CK19 mouse monoclonal antibody (DAKO), and rabbit polyclonal anti-albumin antibodies (Cell Signaling Technology), respectively.

Cell proliferation and colony formation assay

For cell proliferation assays, 2×10^3 cells were seeded in 96-well plates and cultured with 1% FBS DMEM (control), 1% DMEM with OSM (100 ng/mL), 5-FU (2 μg/mL), or OSM (100 ng/mL) and 5-FU (2 μg/mL) for 3 to 7 days without media changes. Cell viability was evaluated in quadruplicate using a CellTiter 96 AQueous kit (Promega). For colony formation assays, 1×10^3 cells were harvested in a one-well Culture Slide (BD Biosciences) and cultured with 1% FBS DMEM (control) with or without OSM (100 ng/mL). Culture medium was replaced every 3 days and the colonies were fixed with ice-cold 100% methanol and used for immunofluorescence 10 days after the initiation of treatment.

RNA interference

SiRNAs specific to OSMR (Silencer Select siRNA S17542) and a control siRNA (Silencer Select Negative Control no. 1) were obtained from Ambion (Applied Biosystems). To each well of a six-well plate, 2×10^5 cells were seeded 12 hours before transfection. Transfection was performed using LipofectAMINE 2000 (Invitrogen), according to the instructions of the manufacturer. A total of 100 pmol/L of siRNA duplex was used for each transfection.

Apoptosis assay

Cells were cultured in 1% FBS DMEM (control), 1% FBS DMEM with OSM (100 ng/mL), 5-FU (2 μg/mL), or OSM (100 ng/mL) and 5-FU (2 μg/mL) for 3 days in six-well plates or in culture slides (BD Biosciences). Annexin V binding to cell membranes was visualized using Annexin V-FITC antibodies and a FACSCalibur flow cytometer (BD Biosciences). Activation of caspase 3 was visualized by immunohistochemistry or immunofluorescence using anti-active caspase-3 polyclonal antibodies (Promega), as described by the manufacturer.

Animal studies

Six-week-old NOD/SCID mice (NOD/NCrCRl-*Prkdc*^{scid}) were purchased from Charles River Laboratories, Inc. The protocol was approved by the Kanazawa University Animal Care and Use Committee. One million tumor cells were suspended in 200 μL of DMEM and Matrigel (1:1), and a s.c. injection was performed. The incidence and size of subcutaneous tumors were recorded. Intratumoral injections of 50 μL of PBS (control), OSM (2 μg/tumor), 5-FU (250 μg/tumor), or OSM (2 μg/tumor) and 5-FU (250 μg/tumor) were initiated twice weekly 48 days after the injection of tumor cells when the average volume of four tumors in each group had reached 400 mm^3. For histologic evaluation, tumors were formalin-fixed and paraffin-embedded.

Statistical analyses

The association of OSMR expression and clinicopathologic characteristics in HCC was examined using either Mann-Whitney U or χ^2 tests. Student's t test was used to compare various test groups assayed by quantitative reverse transcription-PCR analysis. All analyses were performed using GraphPad Prism software.

Results

Distinct expression of OSMRs in HCC

Before exploring the effect of OSM on HCC, we examined the expression of its receptor, OSMR, in surgically resected HCC and adjacent noncancerous liver tissues by immunohistochemistry. Representative staining of OSMRs in tumor/nontumor tissues is shown in Fig. 1A. In general, cell surface and cytoplasmic immunoreactivity to OSMR were rarely detected in hepatocytes in chronic hepatitis liver (a), but were frequently detected in small hepatocyte-like cells in the stroma or transitional cells in the lobule of cirrhotic liver (b), as indicated by the arrows. Note that immunoreactivity to OSMR was not detected in bile duct epithelia or ductular reactions in which EpCAM+ hepatic progenitor cells are thought to accumulate (Supplementary Fig. S1), suggesting that OSMRs might be expressed in hepatic progenitor cells committed to hepatocytes. Immunoreactivity to OSMRs was more strongly detected in HCC than in noncancerous liver (c), and the expression was heterogeneous in the tumor. Of note, OSMRs were detected in HCC cells at the invasive front area of the tumor (d) where CSCs are known to invade frequently (arrows).

Immunoreactivity to OSMR antibodies and EpCAM antibodies was detected in 66 (61.7%) and 38 (35.5%) of 107 HCC specimens, respectively. The clinicopathologic characteristics of OSMR+ and OSMR− HCC cases are shown in Table 1. OSMR+ HCC was characterized by high serum AFP values ($P = 0.009$), poorly differentiated morphology ($P < 0.0001$), and a high frequency of EpCAM+ HCCs ($P = 0.024$), suggesting that the OSMR is expressed in HCC with stem/progenitor cell features. OSMR+ HCC was also characterized by young onset of disease and male dominance, although these features did not reach statistical significance ($P = 0.052$ and 0.058, respectively). OSMR was more frequently detected in EpCAM+ HCCs (76.3%) than in EpCAM− HCCs (53.7%). Expression of OSMR and EpCAM was further investigated by double immunofluorescence analysis, and immunoreactivity to OSMR was detected in both EpCAM+ normal hepatic progenitors (Fig. 1B) and EpCAM+ HCC cells (Fig. 1C). These data suggest that although OSMR is more widely expressed than EpCAM in HCC, OSMR is frequently expressed in EpCAM+ normal hepatic progenitors and liver CSCs.

OSM induces hepatocytic differentiation of EpCAM+ HCC

Because OSMR was expressed in the majority of EpCAM+ HCCs, we investigated the effect of OSM on EpCAM+ HCC cell lines. First, we examined the expression of OSMR and its signal transducer glycoprotein 130 (gp130) in EpCAM+ AFP+ HCC cell lines HuH1 and HuH7 by immunofluorescence

Published OnlineFirst May 18, 2010; DOI:10.1158/0008-5472.CAN-09-4210

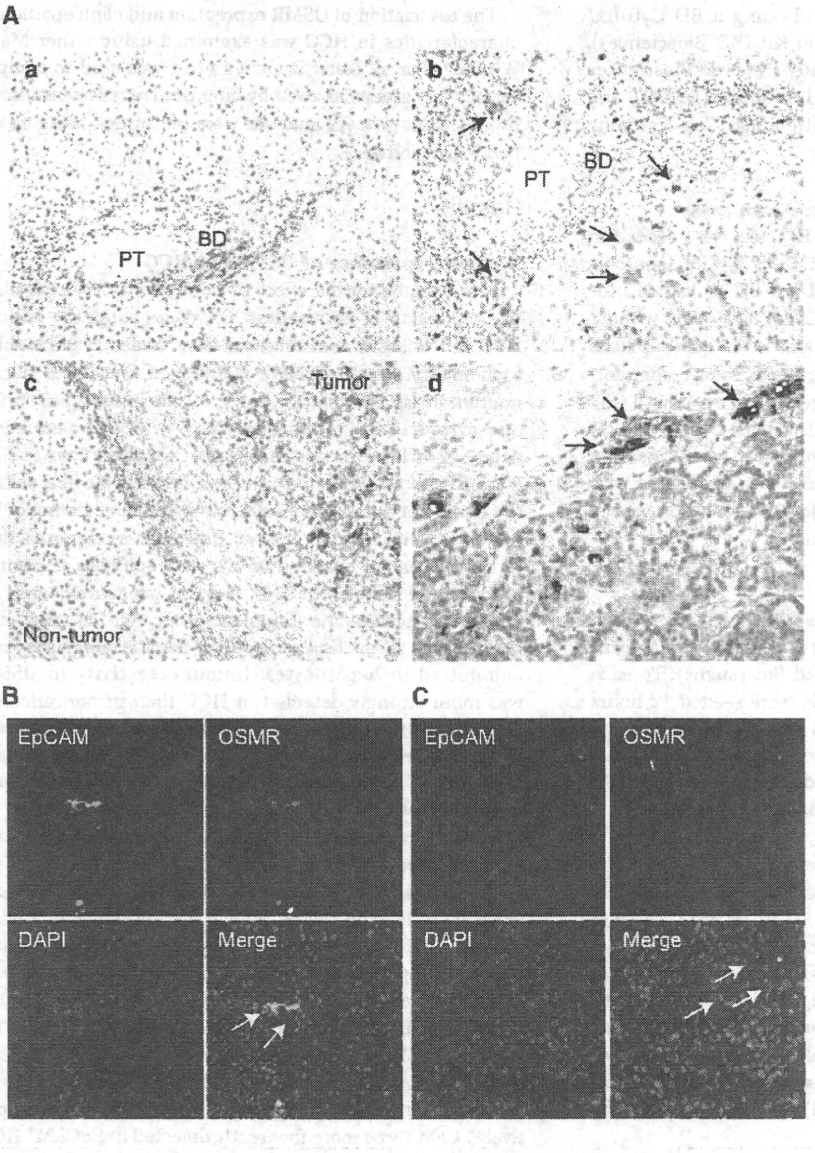

Figure 1. A, representative images of OSMR staining in noncancerous liver tissues and HCC tissues. Immunoreactivity to OSMR was not detected in hepatocytes in chronic hepatitis liver tissue (a) but was detected in a subset of small hepatocyte-like cells in the stroma or transitional cells in the lobule (b, arrows) of cirrhotic liver tissue. OSMR was more abundantly expressed in HCC than in noncancerous liver (c). OSMR$^+$ cancer cells were disseminated in the invasive front area of the tumor (d, arrows). PT, portal tract; BD, bile duct. B and C, double immunofluorescence analysis of EpCAM (green) and OSMR (red) expression in noncancerous (B) and HCC (C) tissues.

(Fig. 2A). Both gp130 and OSMR protein expressions were detected in these cells, consistent with the immunohistochemical data. Because OSM is known to induce the hepatocytic differentiation of hepatoblasts in a STAT3-dependent manner, we investigated the effect of OSM on phosphorylation of STAT3 in HuH1 and HuH7 cells by immunofluorescence and Western blotting. Incubation of HCC cells for 1 hour with OSM at a concentration of 100 ng/mL resulted in the induction and nuclear accumulation of phosphorylated STAT3 compared with controls (Fig. 2B and C). We examined the effect of OSM on the EpCAM$^+$ cell population in HuH1 and HuH7 cells. We first labeled HuH1 and HuH7 cells with CD326 (EpCAM) MicroBeads and FITC-conjugated anti-EpCAM antibodies (Clone Ber-EP4) and performed positive/negative selection using magnetic activated cell sorting to determine the appropriate gating criteria for EpCAM-high (designated as EpCAM$^+$) and EpCAM-low/negative (designated as EpCAM$^-$) cell population (Fig. 2D, top). It is interesting that OSM treatment (100 ng/mL for 72 hours) diminished the EpCAM$^+$ cell population from 50.7% to 10.1% in HuH1 and from 55.2% to 28.8% in HuH7 cells when the same constant gating criteria was applied (Fig. 2D, bottom).

We used RNA interference to investigate whether the decrease in EpCAM$^+$ cells by OSM treatment depends on the expression of OSMR. Transfection of siRNAs specific to *OSMR* (si-OSMR) resulted in the knockdown of target genes

Published OnlineFirst May 18, 2010; DOI:10.1158/0008-5472.CAN-09-4210

compared with the control (si-Control) in HuH1 and HuH7 cells 48 hours after transfection (Supplementary Fig. S2A). We further confirmed the decrease of OSMR protein expression by immunofluorescence and Western blotting 72 hours after transfection (Supplementary Fig. S2B and C). When we treated these HuH1 and HuH7 cells with OSM (100 ng/mL) for 1 hour, we observed the decrease of phosphorylated STAT3 by *OSMR* gene silencing compared with the control (Supplementary Fig. S2C). Furthermore, OSM-mediated decrease in the number of EpCAM$^+$ cells was inhibited by *OSMR* gene silencing (Supplementary Fig. S2D), suggesting that OSM exploits the diminution of EpCAM$^+$ cells through the activation of the OSMR signaling pathway in EpCAM$^+$ HCC.

We further examined the effect of OSM on hepatocytic differentiation by quantitative reverse transcription-PCR and fluorescence-activated cell sorting (FACS) analyses. OSM treatment in HuH1 cells reduced the expression of hepatic progenitor–related genes including *AFP, KRT19* (encoding CK19), and *TERT* (encoding telomerase reverse transcriptase; TERT; Fig. 3A). OSM treatment further reduced the expression of *BMI1* and *POU5F1* (encoding Oct4), which is known to be expressed and required for self-renewal in embryonic stem cells. OSM treatment also increased the expression of the hepatocyte marker, *CYP3A4*. Furthermore, OSM treatment reduced AFP$^+$ and CK19$^+$ cells and increased albumin$^+$ cells compared with the untreated controls, as evaluated by the geometric mean of the fluorescence intensities of whole cells analyzed by intracellular FACS (Fig. 3B). Similar results were obtained in HuH7 cells (data not shown) and, taken together, these data suggest that OSM induced the hepatocytic differentiation of EpCAM$^+$ HCCs.

Hepatocytic differentiation of EpCAM+ HCC by OSM augments cell proliferation

In general, normal stem cells are more quiescent than differentiated cells in terms of cell division. We therefore evaluated the effect of OSM on cell proliferation in HuH1 and HuH7 cells. It is interesting that OSM treatment for 10 days resulted in a larger colony formation following treatment with OSM (100 ng/mL) compared with untreated controls. Of note, the majority of cells comprising these larger colonies were EpCAM$^-$, or had low expression levels, whereas a subset of untreated control cells maintained high EpCAM expression (Fig. 3C). Similar results were obtained when cell proliferation was examined using a [3-(4, 5-dimethylthiazol-2-yl)-5-(3-carboxymethoxyphenyl)-2-(4-sulfophenyl)-2H-tetrazolium] tetrazolium assay and Ki-67 labeling index (Fig. 3D). OSM modestly enhanced cell proliferation (top) and increased Ki-67–positive cells (middle and bottom) compared with untreated controls in both HuH1 and HuH7 cells with statistical significance (Fig. 3D).

OSM treatment increases chemosensitivity of EpCAM+ HCC

The abovementioned data imply that although OSM may induce the hepatocytic differentiation of dormant EpCAM$^+$ liver CSCs, OSM treatment alone might instead enhance cell proliferation through expansion of amplifying differentiated cancer cells *in vitro*, raising the question of efficacy of differentiation therapy in EpCAM$^+$ HCC. Because rapidly amplifying cells are considered to be more sensitive to chemotherapeutic agents, we investigated the effect of combining OSM treatment with conventional chemotherapy to target both dormant CSCs and amplifying non-CSCs. We have shown that 5-FU treatment

Table 1. Clinicopathologic characteristics of OSMR$^+$ and OSMR$^-$ HCC cases used for immunohistochemical analyses

Variables	OSMR$^+$ (n = 66)	OSMR$^-$ (n = 41)	P*
Age (years, mean ± SE)	62.7 ± 1.3	66.4 ± 1.3	0.052
Sex (male/female)	55/11	27/14	0.058
Etiology (HBV/HCV/other)	25/35/6	8/30/3	0.10
Liver cirrhosis (yes/no)	43/23	26/15	1.0
AFP (ng/mL, mean ± SE)	6,453 ± 5901	1,039 ± 935	0.009
Histologic grade†			
I–II	3	16	
II–III	54	20	
III–IV	9	5	<0.0001
Tumor size (<3 cm/>3 cm)	30/36	15/26	0.42
Tumor-node-metastasis classification			
I/II	48	31	
III/IV	18	10	0.82
EpCAM (positive/negative)	29/37	9/32	0.024

*Mann-Whitney U test or χ^2 test.
†Edmondson-Steiner.